Were Neoarchean atmospheric methane hazes and early Paleoproterozoic glaciations driven by the rise of oxygen in surface environments?

Anshuman Swain[1]*, Alan J Kaufman[2], Marcin Kalinowski[3] and William F Fagan[1]

[1]Department of Biology, University of Maryland, College Park, MD 20742, USA

[2]Department of Geology and Earth System Science Interdisciplinary Center, University of Maryland, College Park, MD 20742, USA

[3]Faculty of Physics, University of Warsaw, Pasteura 5, 02-093 Warsaw, Poland

Abstract

Insofar as methane was the predominant greenhouse gas of the Archean and early Proterozoic eons, its wax and wane in Earth's atmosphere would have contributed to climate change and the relative flux of harmful UV radiation to surface environments. If correct, understanding the first-order environmental controls (e.g., O_2 or resource concentration) of the biological methane cycle might shed light on the repetition of biological, atmospheric and climatic events preserved in the sedimentary rock record between ~2.8 and 2.0 billion years ago. Environmental controls on the dynamics of methane cycling may further explain other repetitious events in deep time, as well as the present-day increase in the methane flux to the atmosphere from wetland environments. In this study, we developed an ecological interaction model to predict the conditions in which methane is preferentially released to the atmosphere, and found that the interplay of resource and O_2 availability can cause complex cyclic patterns in methane dynamics that are unrelated to the size and efficiency of any of the microbial communities, to initial conditions, or to other model constraints. Based on these model results, we propose that the cyclicity of methane haze events and glacial episodes in the late Archean and early Proterozoic may have been linked to the progressive increase in oceanic and atmospheric O_2 through the interval.

Keywords: Methane haze, methanogenesis, microbial interaction, oxygen, oscillations

*Corresponding author: answain@terpmail.umd.edu; Address: 3205, Biology-Psychology Bldg., University of Maryland, College Park, MD 20742, USA

Introduction

Like Titan, Saturn's orange-shrouded moon, the early Earth may have been episodically enveloped in a thick blanket of atmospheric methane (CH_4), a powerful greenhouse gas produced by archaeal methanogens in anoxic environments. While the depth and distribution of the CH_4 haze (Pavlov et al., 2001; Zerkle et al., 2012; Izon et al., 2015; 2017) during such events likely varied across the planet due to vertical atmospheric motion and mixing (Wolf and Toon, 2010), the biogenic gas would nonetheless have warmed the troposphere, and through attenuation of the solar UV flux, protected surface environments from high energy radiation.

Carbon isotope evidence from Neoarchean (2.8 to 2.5 billion years ago) organic matter preserved in sedimentary rocks (Eigenbrode and Freeman, 2006) suggests an increase in the methanogenic production of CH_4 and its consumption by methanotrophs to form biomass. Depending on the leak rate of the greenhouse gas from anoxic sediments, CH_4 may have accumulated in sufficient concentrations in the atmosphere to form periodic hazes. The extent and depth of such hazes is likely to have been modulated by the photosynthetic production and accumulation of molecular oxygen (O_2) in the oceans and atmosphere.

Due to the rapid oxidation of CH_4 to CO_2 in the presence of O_2 (Saunois et al., 2016), the atmospheric concentration of methane is generally thought to represent a balance between source and sink reactions. Tipping the scales between the two would thus modulate the size of the atmospheric reservoir. On the source side, the production of CH_4 could have been affected by competition for critical metabolic substrates between methanogens and sulfate reducers, or by the lack of key metal cofactors, like nickel, required for methanogenic enzymes (Anbar and Knoll, 2002; Konhauser et al., 2009). In this analysis, however, we consider ecological factors and biological interactions that may have increased the methane flux from surface environments that are directly associated with the release of photosynthetic O_2. Such a scenario would be particularly relevant in the Neoarchean when periodic CH_4 hazes are suggested from geochemical measurements of sedimentary rocks and photochemical models (Zerkle et al., 2012; Farquhar et al., 2013; Izon et al., 2015; 2017, Williford et at., 2016).

Our dynamic resource-driven model for methane generation is based upon the metabolic repercussions of the Warburg Effect (see Swain and Fagan, 2018), which was initially proposed to explain

uncontrolled cellular proliferation during cancer growth (Warburg, 1956), to an ecological scenario appropriate to Neoarchean and early Paleoproterozoic surface environments and atmospheric fluctuations. The Warburg Effect describes a shift in metabolic respiration where the energetic process of oxidative phosphorylation (OP), which produces CO_2 as an end product, is replaced by glycolysis that instead generates products that can be incorporated into biomass but yields 10 times less energy. This shift in respiration mechanisms is particularly pronounced during the rapid growth of microbial cells that are not resource limited – even in the presence of oxygen. This metabolic phenomenon has been observed in a wide variety of organisms such as bacteria (where it is termed “overflow metabolism”; Basan et al., 2015, Schuster et al., 2015; Zhuang et al., 2011), yeast (the “Crabtree effect”; Deken, 1966), and a diversity of human cells, including Kupffer and microglial cells (specialized macrophages in the liver and brain, respectively), lymphocytes (white blood cells), and fast twitch muscle fibers (Schuster et al., 2015; Vander Heiden et al., 2009). While the Warburg Effect may seem energetically counterintuitive, one can observe that as cells grow rapidly, the kinetic advantage of glycolysis that occurs in the cytoplasm results in a two-fold energy advantage over OP, which is restricted to the cell membrane (Voet and Voet, 2004). Past models thus describe a metabolic arms race between OP and glycolysis that includes: i) efficiency vs. rate (OP is more efficient, but glycolysis is faster), ii) surface area vs. volume (glycolysis occurs in the cell interior whereas OP is constrained to the cell surface), and iii) biomass production (glycolysis produces organic substrates that can be used in biomass production directly, which is generally not true for OP) (see Swain and Fagan, 2018; Schuster et al., 2015). Results from these models suggest that large inputs of resources (any carbon substrate that allows the microbes to grow) with even small inputs of oxygen can stimulate glycolysis over the more energetic process of OP, and therefore, can affect ecological processes, specifically methanogenesis, that use these glycolytic overflow products (e.g., formate, lactate, and acetate).

To understand the dynamics of how resource and O_2 availability can affect the production and consumption of methane, we present a simplified ecological/population interaction ODE (ordinary differential equation) model, using the concept of overflow metabolism associated with the Warburg Effect. The ecological interactions described in this model and its results may be relevant to geological and ecological episodes where pulsed resource inputs or the availability of O_2 can alter the CH_4 production rate.

Our ODE model might then apply to climatic and environmental perturbations of the early Earth, including the cyclic patterns of Neoarchean CH_4 haze events (Pavlov et al., 2001; Zerkle et al., 2012; Izon et al., 2015; 2017) and early Paleoproterozoic glacial episodes (e.g., Bekker and Kaufman, 2007), Neoproterozoic ice ages (Hoffman et al., 1998; Halverson et al., 2002), Phanerozoic mass extinctions (Rothman et al., 2014), and global warming associated with CH_4 fluxes from present-day wetland environments (Saunois et al., 2016).

In our ecological/population interaction model, we focus on five major classes of microbes: aerobic heterotrophic bacteria (A), methanogens (B), aerobic methanotrophs (C), generalized fermenters (F) and anaerobic methanotrophic microbial consortia (G; also known as anaerobic oxidation of methane (AOM) consortia). All of these microbial classes are are involved in the production and/or consumption of generalized resources (R), glycolytic/fermentation products (FP), O_2, CH_4, and CO_2 (**Fig. 1**)

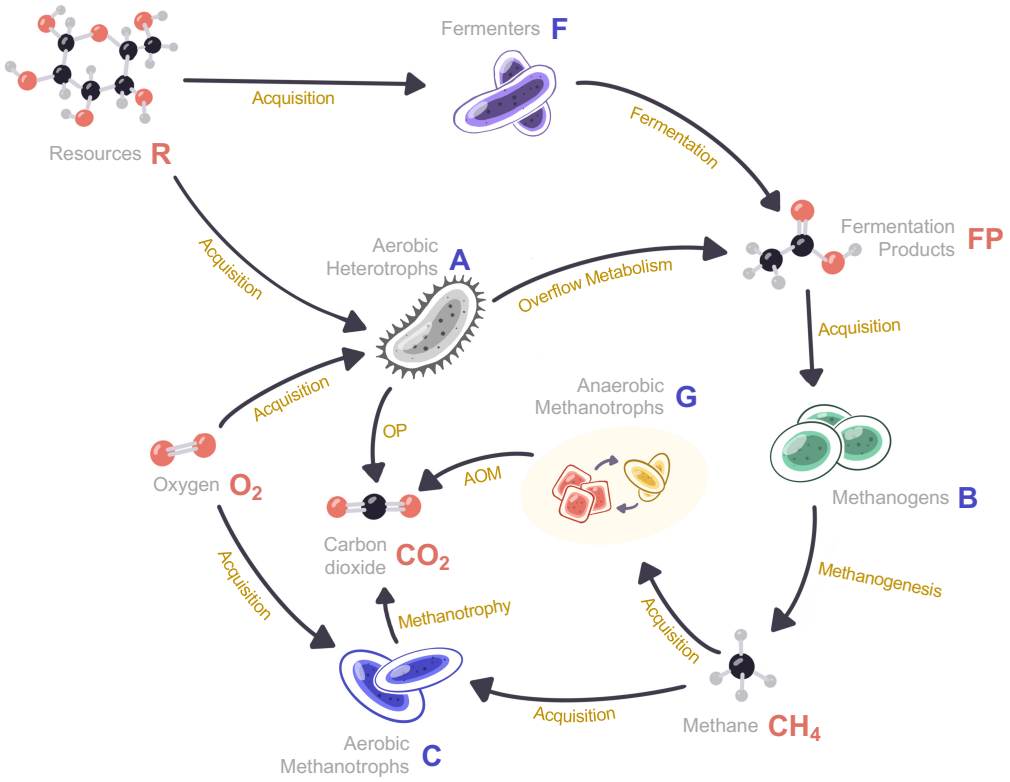

Figure 1: Flow diagram representation of the model system. Here (in blue) A, B, C, F and G are populations of heterotrophic bacteria, methanogens, aerobic methanotrophs, fermenters and anaerobic methanotrophs, respectively. The flux arrows indicate processes that produce (in red) either metabolic

reactants or gases cycled among the microbial consortia. Ordinary differential equations with detailed explanations representing this dynamical system appear in **Methods**.

Fermenters (F) in our model produce simple organic substrates (formate, lactate, and acetate) as do aerobic heterotrophic bacteria (A) through overflow metabolism, insofar as this population responds to increasing R by producing more FP than CO_2, and thereby stimulating methanogenesis (see **Methods**). Methane is consumed by aerobic methanotrophs (C) that utilize O_2 to produce CO_2, and by anaerobic methanotrophs (G), in consortia with various other classes of microbes, to produce either alkalinity or CO_2 through the anaerobic oxidation of methane (AOM). Changes in the size of microbial populations are modelled as functions of the availability of R and the efficiency of their utilization (energy production), as well as their basal energy requirements necessary to maintain homeostasis (energy requirement).

The main rationale behind constructing this coupled ODE-based ecological model is to understand the response of these microbial classes to the availability of R and O_2, through mutual interactions and usage of substrates. Changes in the abundance of resources, metabolic products (FP, CH_4, and CO_2), and O_2 associated with consortia interactions are functions of efficiencies of i) overflow metabolism, ii) respiration, and iii) biomass production and maintenance, as well as the rate of addition of both resources and O_2. First, we performed a series of model explorations in a non-driven state for the coupled ODEs (referred to as non-driven dynamics), where the system (microbes and resources) start from an initial condition and are closed off to external changes (such as R and O_2 addition). After modelling the basic dependence of metabolic parameters and species interactions in closed systems, we investigate the effects of constant R and O_2 additions into an open system (referred to as driven dynamics). Based on our ODE model simulations, we consider this new dynamic perspective to explain the episodic nature of Neoarchean methane haze events and early Paleoproterozoic glaciation.

Results

<u>No external forcing</u>

For the case of no external forcing (non-driven), where the only initial inputs were R and O_2, we ran 500,000 model simulations to steady-state (**Figure S1**). Across these simulations we varied key model

129 parameters (the efficiency of various metabolic reactions, including methanogenesis, AOM, and
130 fermentation) and initial conditions (starting populations of different microbial classes, and original
131 abundance of R and O_2) using Latin Hypercube Sampling (LHS; Carnell, 2020) to explore their impacts on
132 final gas (O_2, CO_2, and CH_4) concentrations. We gauged the importance of the different parameters and
133 conditions using partial rank correlation coefficients (PRCC) (see **Methods**), and found that steady-state
134 CH_4 and CO_2 concentrations varied the most based upon the metabolic parameters of methanogens (these
135 included resource incorporation efficiency, resource utilization efficiency, and energy requirement) (**Figure**
136 **S2B,C**). We also discovered that steady state CO_2 concentration varied strongly as a function of the
137 metabolic parameters that controlled anaerobic methanotrophy (or AOM, G) (**Figure S2B**). Steady state O_2
138 concentrations varied as functions of the metabolic parameters of aerobic methanotrophs (C), aerobic
139 heterotrophic bacteria (A), and methanogens (B) (**Figure S2A**). None of the initial conditions that we varied
140 (i.e., starting populations of different microbial classes and initial concentrations of R and O_2) had a high
141 PRCC for any of the stable state gas concentrations **(Figure S3)**, except for the dependence of the final
142 CO_2 concentration on the initial value of O_2 concentration **(Figure S3B)**.

143 Although the steady state gas concentrations varied quantitatively with certain parameters, the
144 qualitative trends that they depicted were relatively invariant across the Latin hypercube sweep of
145 parameter space and initial conditions. **Figure 2** depicts a specific case, where we plot the steady state
146 variations of the proportions of various gases in a closed non-driven system (initialized at biologically
147 relevant base parametrization) due to changes in the methane production efficiency coefficient (β, see Eqs.
148 4, 9, and 11 in **Methods**), which was set at 1%, 10%, and 50%. With increasing efficiency, the system
149 became more anoxic (lower O_2) and less acidic (lower CO_2), while CH_4 concentrations increased, especially
150 at low initial O_2 and high initial R inputs. We recorded similar model responses for variations of all other
151 parameters (See **Figures S4A-O**). However, we noted lower than expected CO_2 concentrations at low
152 initial O_2 inputs for low efficiencies of parameters governing the incorporation and utilization efficiencies of
153 the aerobic heterotrophs (see Eqs. 2, 3, 8, and 10 in **Methods**; and **Figs. S4D and S4H**); these can be
154 attributed to the PRCC dependence of CO_2 on initial O_2 concentration. We also noted a minor deviation in
155 CH_4 concentration at a high initial O_2 input in the Ω simulations for the anaerobic methanotrophs (see Eqs.
156 7 and 10 in **Methods**; **Fig. S4K**); this was attributable to the formation of CO_2 and its dependence on

metabolic parameters of G. These non-linearities arose in cases where the efficiency of usage or of incorporation are either biologically unrealistic or are at the extreme end of what is possible for biological systems (e.g., a very low O_2 affinity for aerobic heterotrophs or a high CH_4 usage efficiency in anaerobic methanotrophs [see Morris and Schmidt 2013; Bowles et al., 2019]). Overall, these results signify that on average the qualitative outputs of our ODE computations remained consistent across the parametrizations and initial conditions in the non-driven setting.

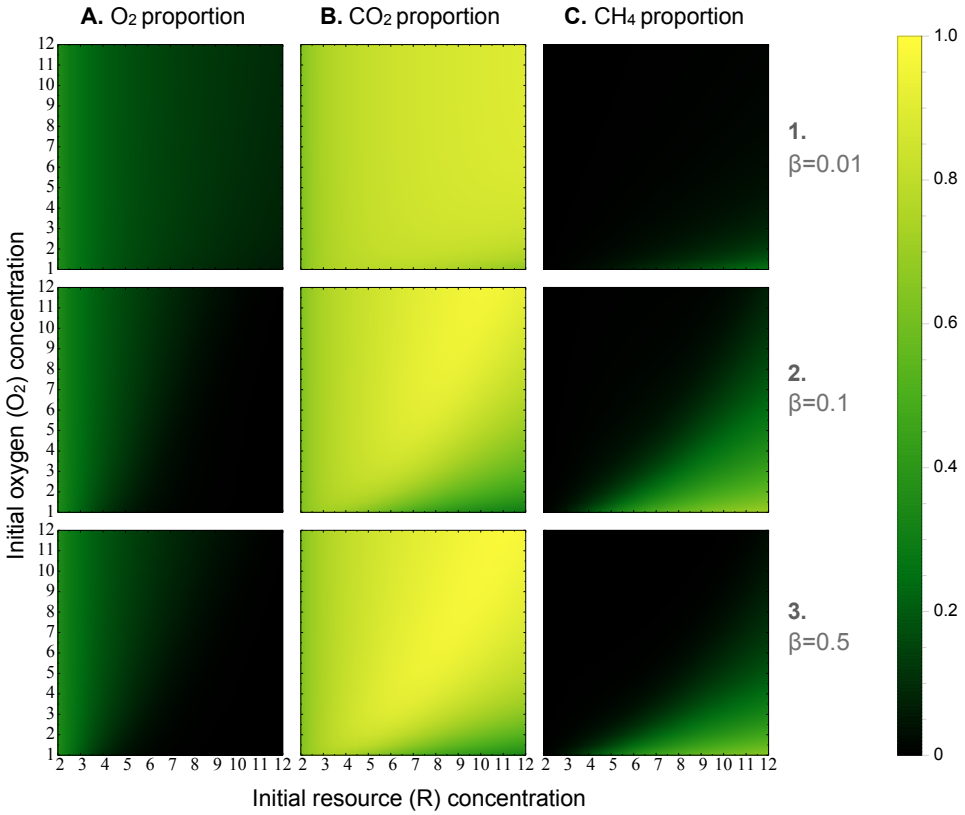

Figure 2: Dynamic variations in O_2, CO_2, and CH_4 proportions (in columns A-C) run to steady state at set O_2 and R input values, with the coefficient of CH_4 production (β) set at 1, 10, and 50% in rows 1-3, respectively. Note that the resource axis begins at 2, due to the constraints posed by minimal energy requirement and below this threshold of basal requirement, all populations die.

<u>External forcing</u>

In contrast with the no forcing scenario above, microbial systems may also be externally forced, particularly by influxes of organic matter (resource, R) and O_2 that are linked through photosynthesis

wherein R is synthesized and O_2 is released as a byproduct of metabolic activity. Model runs with only forced R inputs were qualitatively simple. As illustrated in **Fig. S5**, forcing the model with a constant rate of addition of R depletes O_2 rapidly regardless of its initial abundance. Under these conditions, the Warburg Effect in oxidative heterotrophs does not play a major role in the long-term dynamics of the microbial system. Instead, the Warburg Effect only affects the system initially, so that most FP is derived from general fermenters (F) for the subsequent production of CH_4 through methanogenesis. Notably, simulations with lower initial O_2 (**Fig. S5B**) resulted in an oscillatory behavior over longer periods of CH_4 generation. These results contrast with simulations with higher initial O_2 (**Fig. S5A**), which resulted in quicker damping of the oscillatory behavior. Note, however, that all simulations with the same parameter values reached the same steady state irrespective of the initial conditions, as one can extrapolate from **Figure S5** (and PRCC values from steady state dynamics). Thus, these simulations revealed that differences in the initial O_2 input only affected the timescale of events, as the saturation values (amplitudes) and relative profile shapes of the CH_4, CO_2 and R concentrations remained the same. Higher initial O_2 stabilized the system more rapidly to steady state condition, while higher initial R under low O_2 resulted in sustained oscillations over longer timescales. If the initial R input is held constant, the dynamic solution to forcing the microbial system with a fixed rate of addition of O_2 is that methane will be produced briefly associated with the initial concentration of resource, and O_2 will fall as long as methane is produced and aerobic methanotrophs consume it (**Fig. S6**). After the methane resource is depleted, the continued input of O_2 overwhelms the system and kills the anaerobes, allowing O_2 to increase at a linear rate. Different starting concentrations of R have no apparent effect on system-level dynamics.

Truly complex dynamics occur when both R and O_2 are supplied at constant rates (the input rate per unit time, denoted as $\sigma_1(t)$ for R and $\sigma_2(t)$ for O_2; see Eqs. 8 and 12 in **Methods**) (**Fig. 3).** Low oxygen supply rates relative to resource supply rates (i.e., high $\sigma_1(t)$ / $\sigma_2(t)$ or conversely low $\sigma_2(t)$ / $\sigma_1(t)$) result in large amplitude, slow frequency oscillations in methane and oxygen concentrations in the system, a phenomenon that differs from the model behavior with only resource addition (see **Figure S5; Figure 3A**). With decreasing $\sigma_1(t)$ / $\sigma_2(t)$, these oscillations reduce in amplitude and increase in frequency until a threshold value (of relative O_2 input), where the system reaches a non-oscillatory stable state (**Figure 3A-J; Figure 4**). The transitions into and out of the periodic behavior appear smooth, and the amplitude and

periodicity of the CH_4 peaks within the dynamic interval decline with increasing O_2 input rate. Moreover, the ratio of resource to oxygen input rates at which oscillatory behavior transitions to a stable, non-oscillatory pattern remains constant across the parameter variations and initial conditions (i.e. $\sigma_1(t)/\sigma_2(t) \sim 5$)(**Figure 4B**). **Figure 4A** further illustrates the relationship between the O_2 input rate (σ_2, varied from 10 to 20% of σ_1) on the amplitude and periodicity of CH_4 peaks. Clearly the greatest amplitudes and periods in CH_4 concentration occur at low O_2 input rates, and these both decline rapidly as oxygen overwhelms the system, leading to phase transition when σ_2 is ~ 20% of σ_1 (**Figures 3 and 4**).

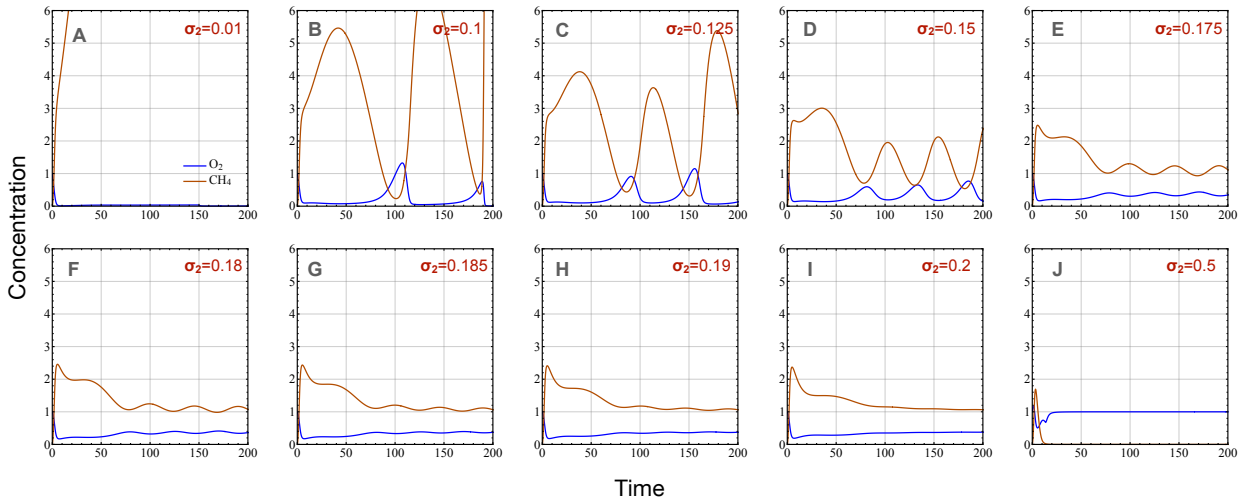

Figure 3: Dynamic variations in O_2 and CH_4 for the externally forced model run with constant rates of addition of R and O_2. The O_2 input rate (σ_2) varied between 1% to 50% relative to the resource input rate across panels (σ_1), but in all cases the R input rate (σ_1) was held constant at 1.

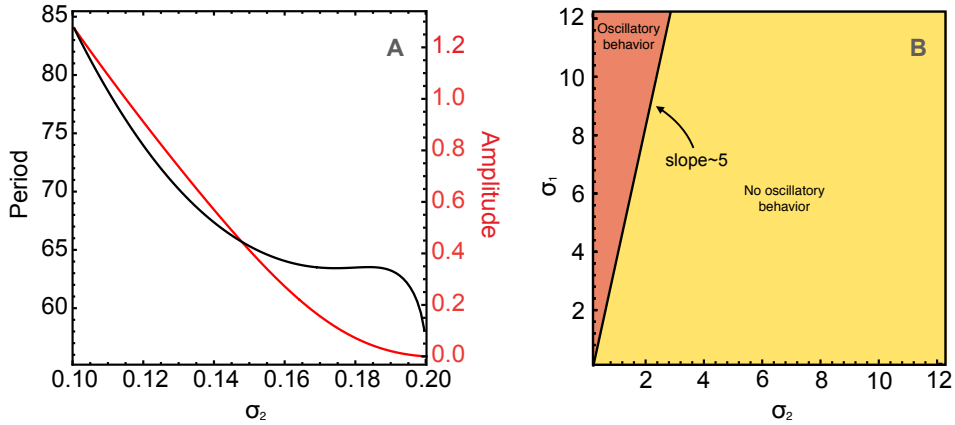

Figure 4: The dependence of amplitude and time period of the CH_4 oscillations in Fig. 3 as a function of the O_2 input rate (σ_2).

Discussion

Our dynamic resource- and population-driven ecological model based on the Warburg Effect reveals clues to the production of CH_4 in response to the availability of molecular O_2 when applied to a system of aerobic and anaerobic microbial consortia. By progressively increasing the input rate of O_2 from 10-20% with respect to the resource input rate, the overflow metabolism of the heterotrophic bacteria provides the resource necessary to produce CH_4 in greater proportions than it is consumed by both aerobic and anaerobic methanotrophs.

Applied to coupled biological and environmental events in deep time, this dynamic ecological model may help to explain how the microbial invention of oxygenic photosynthesis drove fluctuations in the oxidation state of surface environments, as well as the pulsed releases of CH_4 to the atmosphere that formed periodic organic hazes. Carbon isotope compositions of organic matter preserved in sedimentary rocks deposited between ~2.8 to 2.5 billion years ago reveal unprecedented levels of ^{12}C enrichment that are most parsimoniously attributed to the incorporation of biomass formed by methanotrophs (Hayes, 1994; Eigenbrode and Freeman, 2006). Under aerobic conditions, CH_4 is oxidized with molecular O_2 to form biomass through the serine or ribulose monophosphate pathways, and CO_2 (Chistoserdova et al., 2005), where the minimum concentrations of CH_4 and O_2 required to drive the microbial process are estimated at 5-10 μM and 12-20 μM, respectively (Harris and Hanson, 1980; Lidstrom and Somers, 1984). Under anaerobic conditions NO_3^-, NO_2^-, SO_4^{2-}, Fe^{3+}, or Mn^{2+} may also be used to oxidize CH_4 to form simple organic compounds, like acetate, and alkalinity (Yan et al., 2018). If photosynthetically derived resources were high — as expected by the pervasive occurrence of thick organic-rich black shales and carbonates in Neoarchean sedimentary successions worldwide (e.g. Zhelezinskaia et al., 2014) — then almost any local increase in O_2 could have initiated overflow metabolism in extant heterotrophic bacteria. Through microbial community dynamics, this could have resulted in the enhanced release of CH_4 to the atmosphere, as described in the model above. Distributed globally, oceanic oxygen oases could then have been the source of Neoarchean CH_4 hazes.

Independent evidence for the presence of repetitious Neoarchean methane haze events comes from multiple sulfur isotope measurements of pyrite from the same samples where organic matter was

isolated and analyzed. In Neoarchean marginal marine sedimentary successions on multiple continents, geochemical evidence links enhanced methanotrophic biomass inputs in organic-rich sedimentary rocks to the presence of a CH_4 haze that isotopically altered the products of atmospheric SO_2 photochemistry, predominantly sulfate aerosols and elemental sulfur (Kasting, 2001). The photochemical reactions resulted in the mass-independent fractionation, or redistribution, of the sulfur isotope masses (S-MIF) in both of the products that rained down and accumulated in surface environments. Notable negative deviations in the ratio of multiple rare sulfur isotope abundances ($\Delta^{36}S/\Delta^{33}S$) (see **Methods**) relative to normal distribution of Archean S-MIF data (typically referred to as the Archean Reference Array, or ARA) coincide in several discrete stratigraphic intervals with negative excursions in carbon isotope values suggestive of methanotrophic inputs of organic carbon (Zerkle et al., 2012; Farquhar et al., 2013; Izon et al., 2015; 2017, Williford et at., 2016). The most recent of these studies (Izon et al., 2017) used available radiometric constraints to estimate the duration of a single haze event at ~1 million years. Through accelerated H_2 loss to space, the haze events are postulated by these authors to have hastened planetary oxidation. Atmospheric models of Neoarchean hazes suggest that CH_4 concentrations may have been at the level of 20-30 ppm (Zerkle et al., 2012), as opposed to ~2000 ppb in the modern atmosphere. At least three Neoarchean haze events based on these time-series geochemical discoveries are supported by photochemical models that estimate sulfur isotope distributions under different atmospheric CH_4 concentrations (Domagal-Goldman et al., 2008).

While our resource-driven ecological model is neither calibrated for amount nor time, the consistently periodic dynamics of the system under some parameter regimes nonetheless accord with the episodic release of methane from surface environments assuming a constant, but not overwhelming, source of O_2. According to our ecological model, if this oxidant was globally distributed at low concentrations, and if resources were high, a methane haze would likely result. Izon et al. (2017) suggest that the coupled carbon/sulfur isotope anomalies were associated with biospheric responses to increased nutrients, with the CH_4 flux controlled by the availability of organic carbon and sulfate. Increased loading of the oceans with nutrients (e.g., nitrogen, phosphorus) is most often associated with uplift, mountain building and weathering of exposed continental masses, all of which could erode, disrupt, or accelerate sedimentation on marginal marine platforms. In the relatively continuous sedimentary successions where these episodic coupled

anomalies have been recorded, there is no physical evidence for any temporal sedimentary disruption in the form of unconformities or major hiatal surfaces. As an alternative hypothesis, we propose that if nutrients (including ferrous iron, which would have been soluble in the ocean under anoxic conditions) were widely available in the Neoarchean ocean, then the dynamic release of methane and the episodic development of methane hazes in the atmosphere could simply have been the result of constant low level (or gradually increasing) inputs of photosynthetic O_2 to anaerobic environments where overflow metabolism was dominant.

The geochemically documented CH_4 haze events are currently known only from the Neoarchean, but the episodic and potentially globe-encompassing ice ages of the succeeding early Paleoproterozoic Era may similarly be understood in terms of fluctuations of O_2 and greenhouse gases in the ancient atmosphere (Pavlov et al, 2000; Bekker et al., 2005; Kopp et al., 2005; Goldblatt et al., 2006; Claire et al., 2006; Bekker and Kaufman, 2007). Insofar as the early Paleoproterozoic glacial epoch is related to the transition from the anoxic CH_4-rich atmosphere to an oxic CO_2-rich atmosphere, the multiplicity of ice ages (including at least three discrete events) in this interval is arguably related to oscillations in O_2 and CH_4 production and utilization. Related to the dynamic ecological model presented here, the rise of photosynthetic O_2 prior to these Paleoproterozoic glaciations would have progressively drawn down atmospheric methane levels resulting in surface refrigeration. Primary productivity would then be severely limited beneath ice-covered oceans, thereby regulating the production of both fermentative products (FP) and O_2. Atmospheric CO_2 levels during the glaciations likely rose due to unabated volcanic fluxes and limited chemical weathering of exposed continental rocks (e.g., Hoffman et al., 1998). However, once threshold concentrations of CO_2 were reached, the glaciations would end rapidly, resulting in high rates of silicate weathering on land, and the enhanced delivery of sediments, oxidants (including sulfate and nitrate), nutrients, and alkalinity to the oceans. Melting glaciers and sea ice coupled with higher post-glacial temperatures would have flooded continental margins and stimulated both oxygenic photosynthesis and methanogenesis.

Support for such an environmental scenario comes from carbon isotope analyses of drill core samples collected from across the oldest recorded ice age deposit (the Ramsay Lake diamictite) in southern Ontario, which reveal strongly negative $\delta^{13}C$ values (with a nadir of ca. -41‰) in organic matter from sediments that accumulated in the glacial aftermath (Bekker and Kaufman, 2007). The magnitude and

duration of ^{13}C depletion in the post-glacial Pecors Formation (expressed over 100 meters of sedimentary strata) is consistent with long-term methanogenic production and methanotrophic oxidation of CH_4 in a shallow oceanic setting. Multiple rare sulfur isotope abundances in pyrite extracted from the same Pecors samples reveal even more profound negative deviations in $\Delta^{36}S/\Delta^{33}S$ values relative to the ARA (Wing et al., 2002; 2004), which may similarly record atmospheric processes during this (and other) post-glacial early Paleoproterozoic methane haze events. Considering the results of our dynamic ecological model, we suggest that the end of the early Paleoproterozoic glacial epoch around 2.2 billion years ago likely marked the end of extended methane-dominated atmospheres of the early Earth. This repetitive series of ice ages was followed by a remarkably long-lived (>100 million years) interval of highly positive carbon isotope compositions in carbonates known as the Lomagundi-Jatuli event (Karhu and Holland, 1996; Bachan and Kump, 2015; Mänd et al., 2020). Insofar as significant ^{13}C enrichments in marine carbonates are driven by the burial and sequestration of ^{12}C-rich organic matter (Broecker, 1970; Hayes, 1983), the attendant photosynthetic production and release of O_2 at this time would most likely have marked the transition to an oxygenated atmosphere with carbon dioxide acting as the major greenhouse gas.

Episodically enhanced CH_4 release and buildup in the atmosphere later in Earth history may be related to the tectonic reorganization of the mobile continents, which modulate the delivery of reduced gases from spreading ridges and weathering fluxes from uplifted mountains. These variable fluxes would have impacted the photosynthetic production of organic matter and degree of ocean oxygenation during discrete climatic and biological events. Insofar as our model results indicate that these factors control CH_4 fluxes to the atmosphere, we speculate that younger ice ages of the Neoproterozoic and Paleozoic eras, as well as Phanerozoic mass extinctions, may be linked to the dynamic microbial processes modeled here.

Conclusion

The non-driven and driven simulations of CH_4 production and release by a model microbial system suggest that both resources and O_2 play an important role in defining the dynamics of microbial ecosystems over both short and long-time scales. We demonstrate that forced low level inputs of O_2 result in pulsed releases of CH_4 via overflow metabolism, a pattern that may explain periodic CH_4 haze events and episodic glaciation deep in Earth's history. Such pulsed methane releases also occur in modern-day wetlands where

tidal flooding repeatedly tips the balance between oxic and anoxic conditions (see Zhu et al., 2017), suggesting similar mechanisms may be at work. The qualitative behavior of this simple ecosystem model provides a platform for understanding the dynamics of mixed microbial communities in ancient, modern, and future ecosystems. More detailed models that blend empirical gas-release data with calibrated input parameters should shed further light on the links between microbial communities and atmospheric dynamics.

Methods

Modeling Microbial System Dynamics

We model the dynamics of the interacting microbial system as a system of ordinary differential equations (ODEs). First, we define functions pertaining to the Warburg effect (eq. 1-2) and then describe the population evolution equations for each of the microbial consortia.

We begin by defining two functions that describe Warburg Effect dynamics in aerobic heterotrophic bacteria (A):

$$f([R], A) = \begin{cases} \alpha\, A\,([R] - R_0) & \text{for } [R] > R_0 \\ 0 & \text{for } [R] < R_0 \end{cases}$$

Eq. 1 (overflow metabolism of A)

$$g([R], A) = \begin{cases} \varepsilon\, A\, R_1 & \text{for } [R] > R_1 \\ \varepsilon\, A\, [R] & \text{for } [R] < R_1 \end{cases}$$

Eq. 2 (respiratory function of A)

The first function *f*(*R,A*) denotes the process of overflow metabolism, where despite the presence of ample oxygen, heterotrophic aerobic bacteria (A) produce fermentation products when resources are abundant. In this function, at resource concentrations higher than base levels (represented by R_0), there is a linear increase in overflow products (see Basan et al., 2015, Swain and Fagan, 2018). The second function *g*(*R,A*) denotes the respiratory function (see Eq. 3 below) for these organisms (with the maximal resource usage condition represented by resource concentration of R_1). Both α and ϵ are proportionality constants that denote the efficiency of overflow metabolism and respiration, respectively, and fall in the range [0,1].

The differential equations below pertain to changes through time of the dominance of metabolic classes as the different microbial consortia (A, B, C, F, and G as defined in Fig 1) compete for available substrates under variable environmental conditions.

$$\frac{dA}{dt} = (1 - \mu)\,[\mathrm{O_2}]\,g([R], A) - s\,A \qquad \text{Eq. 3}$$

$$\frac{dB}{dt} = (1 - \kappa)\,\beta\,[\mathrm{FP}]\,B - u\,B \qquad \text{Eq. 4}$$

$$\frac{dC}{dt} = (1 - \lambda)\,\gamma\,[\mathrm{O_2}][\mathrm{CH_4}]\,C - v\,C \qquad \text{Eq. 5}$$

$$\frac{dF}{dt} = (1 - \xi)\,\omega\,[R]\,F - a_1\,F \qquad \text{Eq. 6}$$

$$\frac{dG}{dt} = (1 - \psi)\,\Omega\,[\mathrm{CH_4}]\,G - a_2\,G \qquad \text{Eq. 7}$$

The first term on the right side of each differential equation is positive and denotes the process of assimilation of substrates needed for growth (increase in biomass) and energy production for the metabolic class. The second term in each equation is negative and denotes the energy requirement for homeostasis (see Table 1). In equations 3-7, the terms governing resource incorporation efficiency, $\text{generically denoted } (1 - X)$ with X replaced by the consortium-specific parameters $(\mu, \kappa, \lambda, \xi \text{ and } \psi)$,specify the proportion of the required substrate in the extracellular environment that is incorporated into cells, which can then be used for making biomass by that consortium. Variation in these efficiencies is assumed to be modulated by biochemical and physical constraints of the different microbial consortia. The remaining reservoir of resources outside of the cell either leave the system as gases or are available for later incorporation. All ten coefficients of efficiency ($\mu, \kappa, \lambda, \xi, \psi, \varepsilon, \beta, \gamma, \omega, and\ \Omega$) lie in the range [0,1]. The coefficients related to homeostasis ($s, u, v, a_1, or\ a_2$) represent the basal metabolic requirement values for microbial consortia A, B, C, F and G, respectively. All parameters and their interpretations are summarized in Table 1.

Consortium	Resource incorporation efficiency	Resource utilization efficiency	Energy requirements for homeostasis
A (aerobic heterotrophs)	(1 - μ)	ε (for R)	s
B (methanogens)	(1 - κ)	β (for FP)	u
C (aerobic methanotrophs)	(1 - λ)	γ (for O_2 and CH_4)	v

F (fermenters)	(1 - ξ)	ω (for R)	a_1
G (anaerobic methanotrophs)	(1 - ψ)	Ω (for CH_4)	a_2

Table 1: Differential equation parameters governing the dynamics of a system of five microbial consortia. Parameters summarize the efficiency of resource incorporation, the efficiency of resource utilization, and the energy requirements for homeostasis.

The following set of differential equations reflect dynamic changes in the abundance of resources or metabolic products in the five microbial consortia through time:

$$\frac{d[R]}{dt} = -f([R], A) - g([R], A) - \xi\,\omega\,[R]\,F + \sigma_1(t) \qquad \text{Eq 8}$$

$$\frac{d[\mathrm{FP}]}{dt} = f([R], A) - \beta\,B\,[\mathrm{FP}] + \xi\,\omega\,R\,F \qquad \text{Eq 9}$$

$$\frac{d[\mathrm{CO_2}]}{dt} = \mu\,[\mathrm{O_2}]\,g([R], A) + \gamma\,\lambda\,[\mathrm{O_2}]\,[\mathrm{CH_4}]\,C + \psi\,\Omega\,[\mathrm{CH_4}]\,G \qquad \text{Eq 10}$$

$$\frac{d[\mathrm{CH_4}]}{dt} = \kappa\,\beta B\,[\mathrm{FP}] - \gamma\,[\mathrm{O_2}]\,[\mathrm{CH_4}]\,C - \Omega\,[\mathrm{CH_4}]\,G \qquad \text{Eq 11}$$

$$\frac{d[\mathrm{O_2}]}{dt} = -\{\mu\,[\mathrm{O_2}]\,g([R], A) + \gamma\,\lambda\,[\mathrm{O_2}]\,[\mathrm{CH_4}]\,C\} + \sigma_2(t) \qquad \text{Eq 12}$$

In equations 8-12 the positive terms on the right side of the differential equation indicate either input or production of the resources, while negative terms indicate metabolic resource consumption. All the terms involve interaction of the resources with one or more of the microbial consortia, which are modelled in equations 3-7, except for $\sigma_1(t)\ and\ \sigma_2(t)$. These terms (see Eqs. 8 and 12) denote the time-dependent input rates of R and O_2 that are controlled externally. In this model, CO_2 is considered a sink that evades to the atmosphere and is decoupled from the autotrophic processes. This assumption makes R an independent variable, and further ensures that substrate production is not photoautotrophic (the case in many scenarios). Moreover, as developed here the ecological model is not spatially explicit in order to make the results more general in nature.

There exist many methanogenic systems where oxic and anoxic parts are heterogeneously mixed, albeit at generally small scales or temporally, such as in wetlands (Kirsche et al., 2013). In this ecological model we have simplified the process of methanogenesis in several ways: i) FPs can be one of many substrates, including formate, acetate, and lactate, all of which can be used for methane production by

various methanogens; and ii) for hydrogen (H_2) + CO_2 methane production, we assume that reduced reactants are unlimited, and insofar as CO_2 is a sink and evades the system as a gas, it is unlimited as well (i.e., it is not used for autotrophic processes that deliver new resources to the community). For the anaerobic oxidation of methane by population G, we lump all of the potential anaerobic methanotrophs here, but recognizing that both CO_2 and carbonate alkalinity may be formed, we include a conversion efficiency term (Ω) to calculate the relative concentrations of CO_2 alone.

This coupled differential equation system was solved through Wolfram Mathematica v. 12.1 and R v 3.6.2. A regular parameter sweep was first performed for the non-driven case (no external input: $\sigma_1, \sigma_2 = 0$) using Latin Hypercube sampling (LHS) for 500,000 different scenarios using R packages *deSolve* (Soetaert et al., 2010) and *lhs* (Carnell, 2020). We then calculated the partial rank correlation coefficients (PRCCs) to explore the effect of each parameter and initial condition on the concentrations of gases (methane, oxygen and carbon dioxide) through R package *sensitivity* (Iooss et al., 2020).

To further explore the trends in these gas emissions, we calculated the relative proportions of these gases under a set of base parameters that depict biologically possible scenarios (according to data from Payne and Wiebe, 1978; Geyer et al., 2016; Bowles et al., 2019; and Morris and Schmidt, 2013). All the efficiencies were set at half maximum for the base case. We then varied one parameter at a time to look at the dependence on that specific variable on gas emissions as a function of resource and oxygen initial conditions. In doing so, we collated the data for different initial conditions (such as different initial ratios of the microbial consortia), and plotted the averaged values of the equilibrium state as a function of initial resource and oxygen inputs. For driven dynamics, we followed the same procedure of parameter dependence, especially for the two R and O_2 external input parameters, σ_1 and σ_2. To calculate the period and amplitude of the driven dynamics, values were numerically estimated based on dynamic results from the first few oscillations. Periodicity statistics for the dynamics resulting from both high and low extreme values of σ_2 are estimates given the difficulty of estimating them for very long or extremely short oscillations that occur at these values of σ_2.

Notation for Sulfur Isotope Compositions

Sulfur-isotope ratios are conventionally reported in delta (δ) notation and reflect the permil (‰) deviation of the ratio of the least abundant isotope (^{33}S, ^{34}S, or ^{36}S) to the most abundant isotope (^{32}S), relative to the same ratio in an international reference standard (Vienna Canyon Diablo Troilite, V-CDT). For example, $\delta^{34}S = [(^{34}S/^{32}S)_{sample}/(^{34}S/^{32}S)_{V\text{-}CDT} - 1] \times 1000$. The majority of terrestrial processes fractionate S-isotopes mass-dependently, whereby $\delta^{33}S \approx 0.515 * \delta^{34}S$ and $\delta^{36}S \approx 1.91 * \delta^{34}S$. Departure from mass-dependent behavior, or mass-independent fractionation (S-MIF), is expressed in capital-delta (Δ) notation as either non-zero $\Delta^{33}S = [(^{33}S/^{32}S)_{sample}/(^{33}S/^{32}S)_{V\text{-}CDT} - (^{34}S/^{32}S)_{sample}/(^{34}S/^{32}S)_{V\text{-}CDT}]^{0.515}$ or $\Delta^{36}S = [(^{36}S/^{32}S)_{sample}/(^{36}S/^{32}S)_{V\text{-}CDT} - (^{34}S/^{32}S)_{sample}/(^{34}S/^{32}S)_{V\text{-}CDT}]^{1.9}$.

Acknowledgements

This research was supported in part by NSF award EAR-1338810 to AJK. AS would like to thank the COMBINE program at the University of Maryland (DGE-1632976) for technical and academic support.

Code and data availability

All the codes that were used to explore the ODE model and generate the relevant figures are available publicly at the following github repository: https://github.com/anshuman21111/ch4_haze . All extra figures and simulation data, above and exceeding the supplementary materials are also found on this repository.

References

1. Anbar, A.D. and Knoll, A.H., 2002. Proterozoic ocean chemistry and evolution: a bioinorganic bridge?. science, 297(5584), pp.1137-1142.
2. Bachan, A. and Kump, L.R., 2015. The rise of oxygen and siderite oxidation during the Lomagundi Event. Proceedings of the National Academy of Sciences, 112(21), pp.6562-6567.
3. Basan, M., Hui, S., Okano, H., Zhang, Z., Shen, Y., Williamson, J.R. and Hwa, T., 2015. Overflow metabolism in Escherichia coli results from efficient proteome allocation. Nature, 528(7580), pp.99-104.

4. Bekker, A., Kaufman, A.J., Karhu, J.A. and Eriksson, K.A., 2005. Evidence for Paleoproterozoic cap carbonates in North America. Precambrian Research, 137(3-4), pp.167-206.
5. Bekker, A. and Kaufman, A.J., 2007. Oxidative forcing of global climate change: a biogeochemical record across the oldest Paleoproterozoic ice age in North America. Earth and Planetary Science Letters, 258(3-4), pp.486-499.
6. Carnell, R., 2020. lhs: Latin Hypercube Samples. R package version 1.0.2. https://CRAN.R-project.org/package=lhs
7. Chistoserdova, L., Vorholt, J.A. and Lidstrom, M.E., 2005. A genomic view of methane oxidation by aerobic bacteria and anaerobic archaea. Genome biology, 6(2), p.208.
8. Eigenbrode, J.L. and Freeman, K.H., 2006. Late Archean rise of aerobic microbial ecosystems. Proceedings of the National Academy of Sciences, 103(43), pp.15759-15764.
9. Farquhar, J., Cliff, J., Zerkle, A.L., Kamyshny, A., Poulton, S.W., Claire, M., Adams, D. and Harms, B., 2013. Pathways for Neoarchean pyrite formation constrained by mass-independent sulfur isotopes. Proceedings of the National Academy of Sciences, 110(44), pp.17638-17643.
10. Halverson, G.P., Hoffman, P.F., Schrag, D.P. and Kaufman, A.J., 2002. A major perturbation of the carbon cycle before the Ghaub glaciation (Neoproterozoic) in Namibia: Prelude to snowball Earth?. Geochemistry, Geophysics, Geosystems, Vol. 3(6)
11. Hayes, J.M., 1994. Early life on Earth. In Nobel symposium (Vol. 84, pp. 220-36).
12. Iooss, B., Da Veiga, S., Janon, A., Pujol, G., et al., 2020. sensitivity: Global Sensitivity Analysis of Model Outputs. R package version 1.20.0. https://CRAN.R-project.org/package=sensitivity
13. Izon, G., Zerkle, A.L., Zhelezinskaia, I., Farquhar, J., Newton, R.J., Poulton, S.W., Eigenbrode, J.L. and Claire, M.W., 2015. Multiple oscillations in Neoarchaean atmospheric chemistry. Earth and Planetary Science Letters, 431, pp.264-273.
14. Izon, G., Zerkle, A.L., Williford, K.H., Farquhar, J., Poulton, S.W. and Claire, M.W., 2017. Biological regulation of atmospheric chemistry en route to planetary oxygenation. Proceedings of the National Academy of Sciences, 114(13), pp.E2571-E2579.
15. Kasting, J.F., 2001. The rise of atmospheric oxygen. Science, 293(5531), pp.819-820.

16. Kirschke, S., Bousquet, P., Ciais, P., Saunois, M., Canadell, J.G., Dlugokencky, E.J., Bergamaschi, P., Bergmann, D., Blake, D.R., Bruhwiler, L. and Cameron-Smith, P., 2013. Three decades of global methane sources and sinks. Nature geoscience, 6(10), pp.813-823.
17. Konhauser, K.O., Pecoits, E., Lalonde, S.V., Papineau, D., Nisbet, E.G., Barley, M.E., Arndt, N.T., Zahnle, K. and Kamber, B.S., 2009. Oceanic nickel depletion and a methanogen famine before the Great Oxidation Event. Nature, 458(7239), pp.750-753.
18. Kopp, R.E., Kirschvink, J.L., Hilburn, I.A. and Nash, C.Z., 2005. The Paleoproterozoic snowball Earth: a climate disaster triggered by the evolution of oxygenic photosynthesis. Proceedings of the National Academy of Sciences, 102(32), pp.11131-11136.
19. Pavlov, A.A., Kasting, J.F., Eigenbrode, J.L. and Freeman, K.H., 2001. Organic haze in Earth's early atmosphere: Source of low-13C Late Archean kerogens?. Geology, 29(11), pp.1003-1006
20. Saunois, M., Bousquet, P., Poulter, B., Peregon, A., Ciais, P., Canadell, J.G., Dlugokencky, E.J., Etiope, G., Bastviken, D., Houweling, S. and Janssens-Maenhout, G., 2016. The global methane budget 2000–2012. *Earth System Science Data*, *8*(2), pp.697-751.
21. Soetaert, K., Petzoldt, T. and Setzer, R.W., 2010. Package deSolve: solving initial value differential equations in R. J Stat Softw, 33(9), pp.1-25.
22. Swain, A. and Fagan, W.F., 2018. A mathematical model of the Warburg Effect: Effects of cell size, shape and substrate availability on growth and metabolism in bacteria. Math. Biosci. Eng, 16, pp.168-186.
23. Voet, D. and Voet, J.G., 2004. Biochemistry. Hoboken. John Wiley & Sons
24. Warburg, O., 1956. On the origin of cancer cells. Science, 123(3191), pp.309-314.
25. Williford, K.H., Ushikubo, T., Lepot, K., Kitajima, K., Hallmann, C., Spicuzza, M.J., Kozdon, R., Eigenbrode, J.L., Summons, R.E. and Valley, J.W., 2016. Carbon and sulfur isotopic signatures of ancient life and environment at the microbial scale: Neoarchean shales and carbonates. Geobiology, 14(2), pp.105-128.
26. Wing, B.A., Bekker, A., Brabson, L., Farquhar, J., Kaufman, A.J. and Rumble, D., 2004, November. Atmospheric chemistry of SO2 during the earliest Huronian glaciation. In Abstr. Progr. Geol. Soc. Am (Vol. 36).

27. Wing, B.A., Brabson, E., Farquhar, J., Kaufman, A.J., Rumble, D. and Bekker, A., 2002, August. Delta S-33, delta S-34 and delta C-13 constraints on the Paleoproterozoic atmosphere during the earliest Huronian glaciation. In Geochimica et Cosmochimica Acta Vol. 66, No. 15 A, pp. A840-A840
28. Wolf, E.T. and Toon, O.B., 2010. Fractal organic hazes provided an ultraviolet shield for early Earth. Science, 328(5983), pp.1266-1268.
29. Yan, Z., Joshi, P., Gorski, C.A. and Ferry, J.G., 2018. A biochemical framework for anaerobic oxidation of methane driven by Fe (III)-dependent respiration. Nature communications, 9(1), pp.1-9.
30. Zerkle, A.L., Claire, M.W., Domagal-Goldman, S.D., Farquhar, J. and Poulton, S.W., 2012. A bistable organic-rich atmosphere on the Neoarchaean Earth. Nature Geoscience, 5(5), pp.359-363.
31. Zhelezinskaia, I., Kaufman, A.J., Farquhar, J. and Cliff, J., 2014. Large sulfur isotope fractionations associated with Neoarchean microbial sulfate reduction. Science, 346(6210), pp.742-744.

Supplementary figures

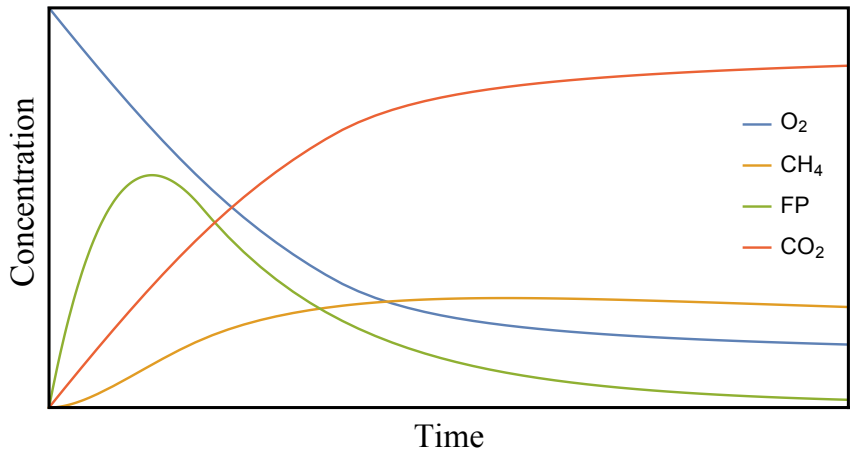

Figure S1: Dynamic variations in O_2, FP, CH_4, and CO_2 through time with set initial boundary conditions so that (relative) concentrations eventually level out when the system reaches steady-state equilibrium, for a non-driven case.

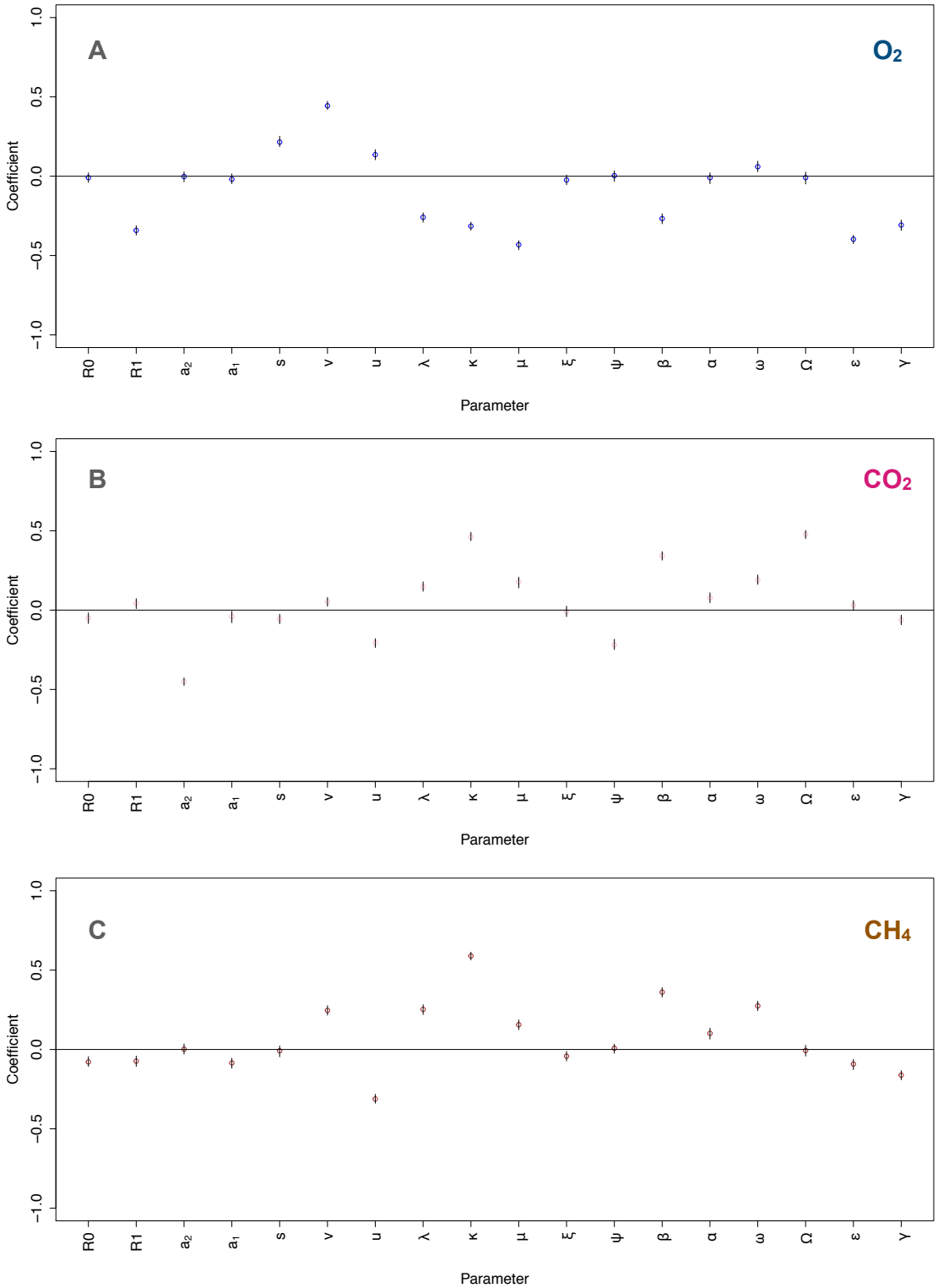

Figure S2: Latin hypercube sampling (LHS) based Partial rank correlation coefficient (PRCC) (which varies from -1 to 1) of the model parameters with respect to the final gas concentrations

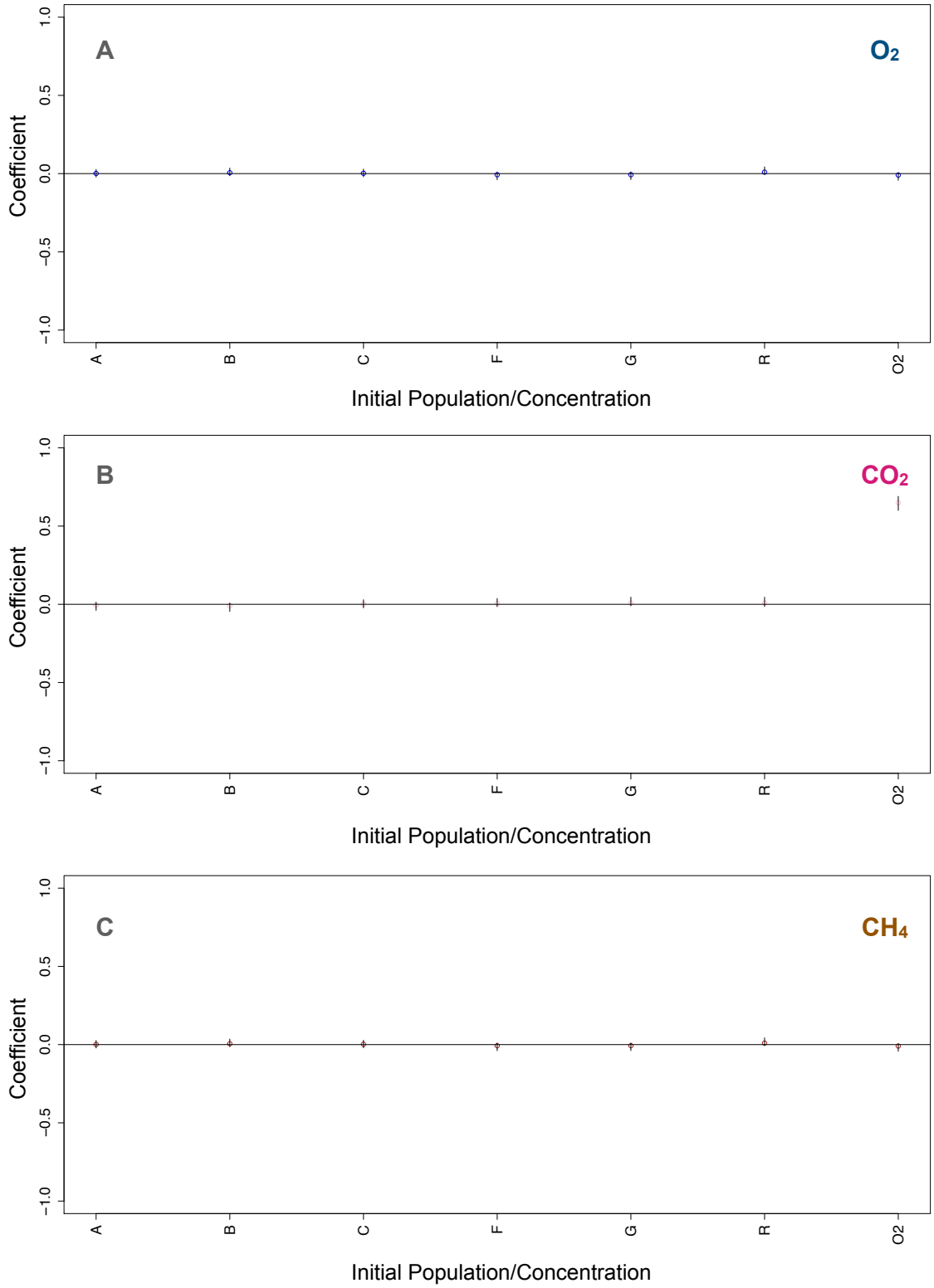

Figure S3: Latin hypercube sampling (LHS) based Partial rank correlation coefficient (PRCC) (which varies from -1 to 1) of the model initial conditions with respect to the final gas concentrations. Please note the extremely small values (absolute value <0.05) of PRCC in all cases except that of CO_2 dependence on O_2 initial value.

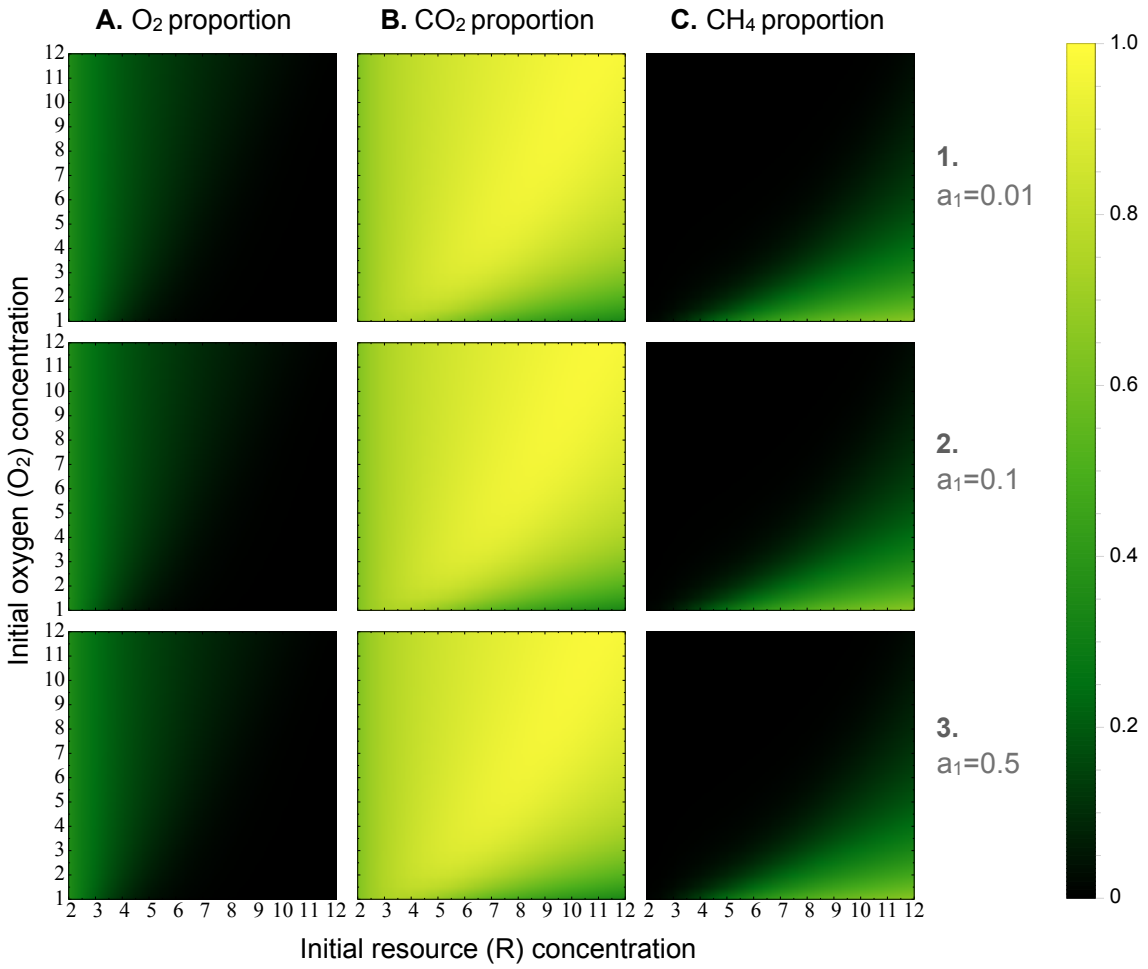

Figure S4A: Variations in O_2, CO_2, and CH_4 proportions (in columns A-C) run to steady state at set O_2 and R input values, with the energy requirement for fermenters (a_1) set at 1, 10, and 50% in rows 1-3, respectively.

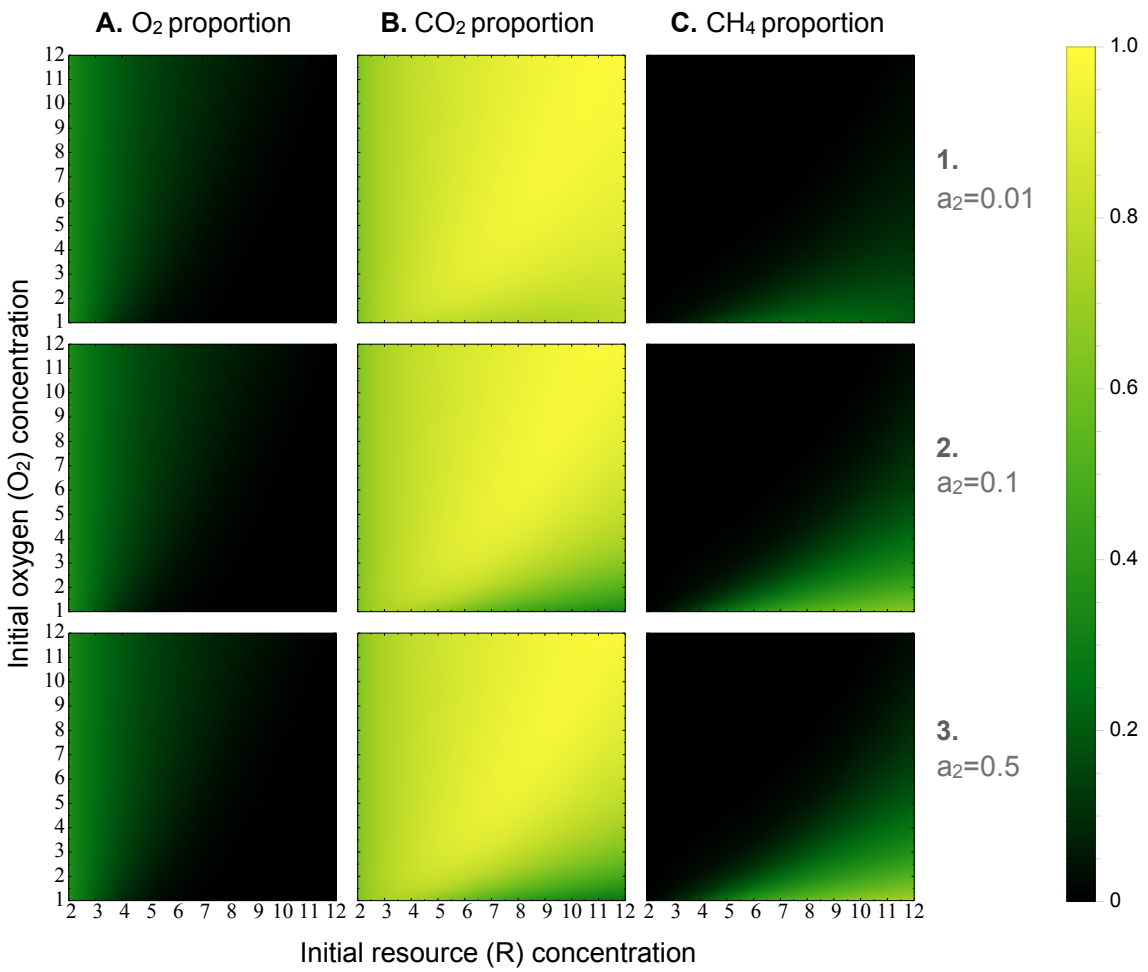

Figure S4B: Variations in O_2, CO_2, and CH_4 proportions (in columns A-C) run to steady state at set O_2 and R input values, with the energy requirement for anaerobic methanotrophs (a_2) set at 1, 10, and 50% in rows 1-3, respectively.

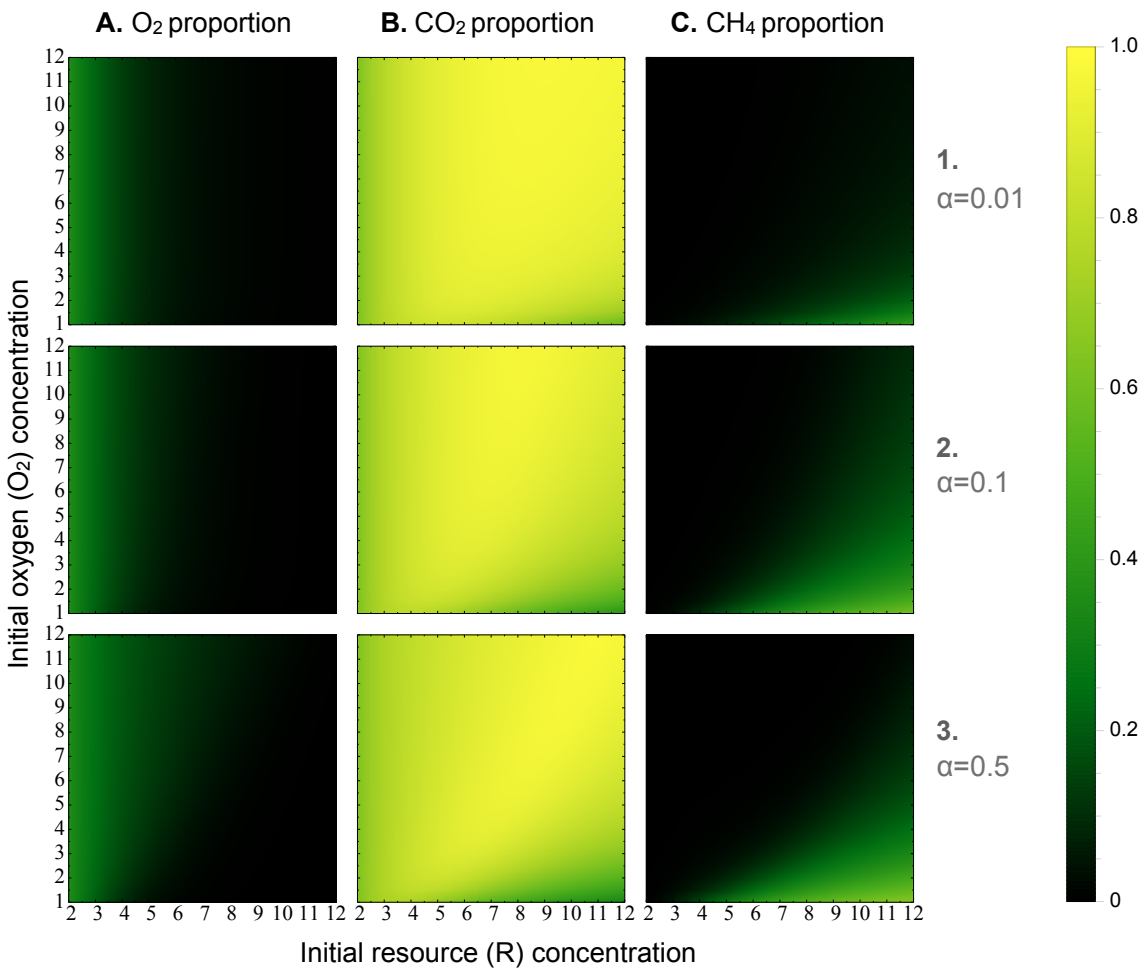

Figure S4C: Variations in O_2, CO_2, and CH_4 proportions (in columns A-C) run to steady state at set O_2 and R input values, with efficiency of overflow metabolism in aerobic heterotrophs (α) set at 1, 10, and 50% in rows 1-3, respectively.

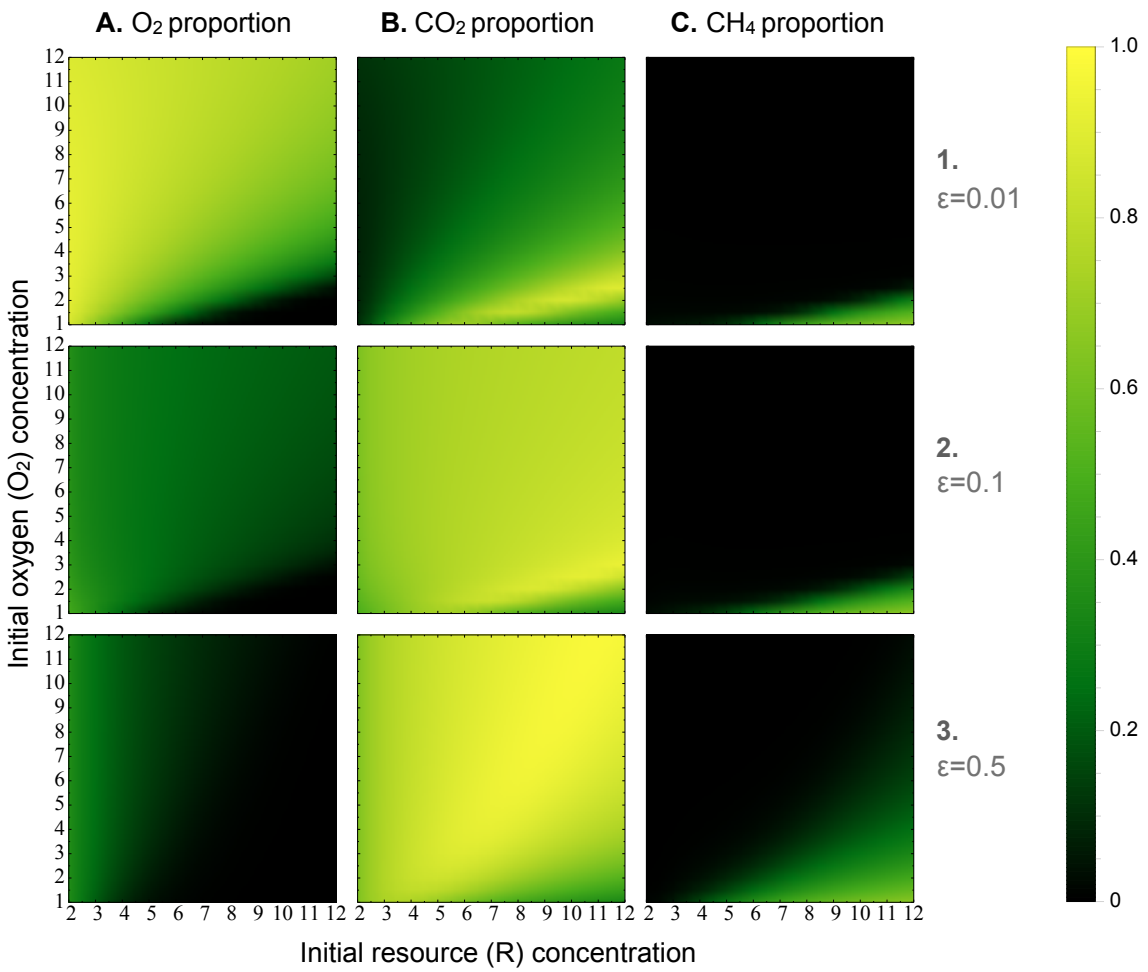

Figure S4D: Variations in O_2, CO_2, and CH_4 proportions (in columns A-C) run to steady state at set O_2 and R input values, with resource utilization efficiency for respiration in aerobic heterotrophs (ε) set at 1, 10, and 50% in rows 1-3, respectively.

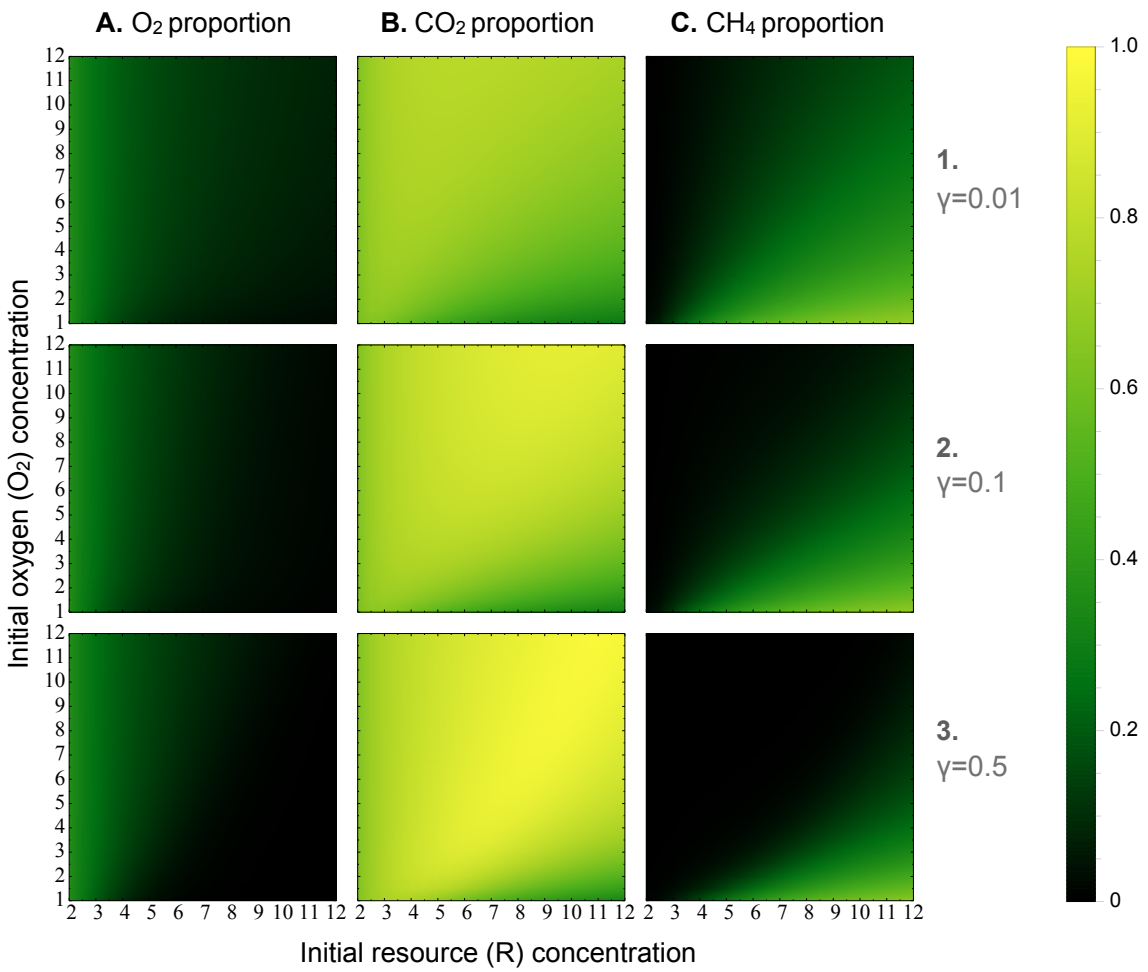

Figure S4E: Variations in O_2, CO_2, and CH_4 proportions (in columns A-C) run to steady state at set O_2 and R input values, with resource utilization efficiency in aerobic methanotrophs (γ) set at 1, 10, and 50% in rows 1-3, respectively.

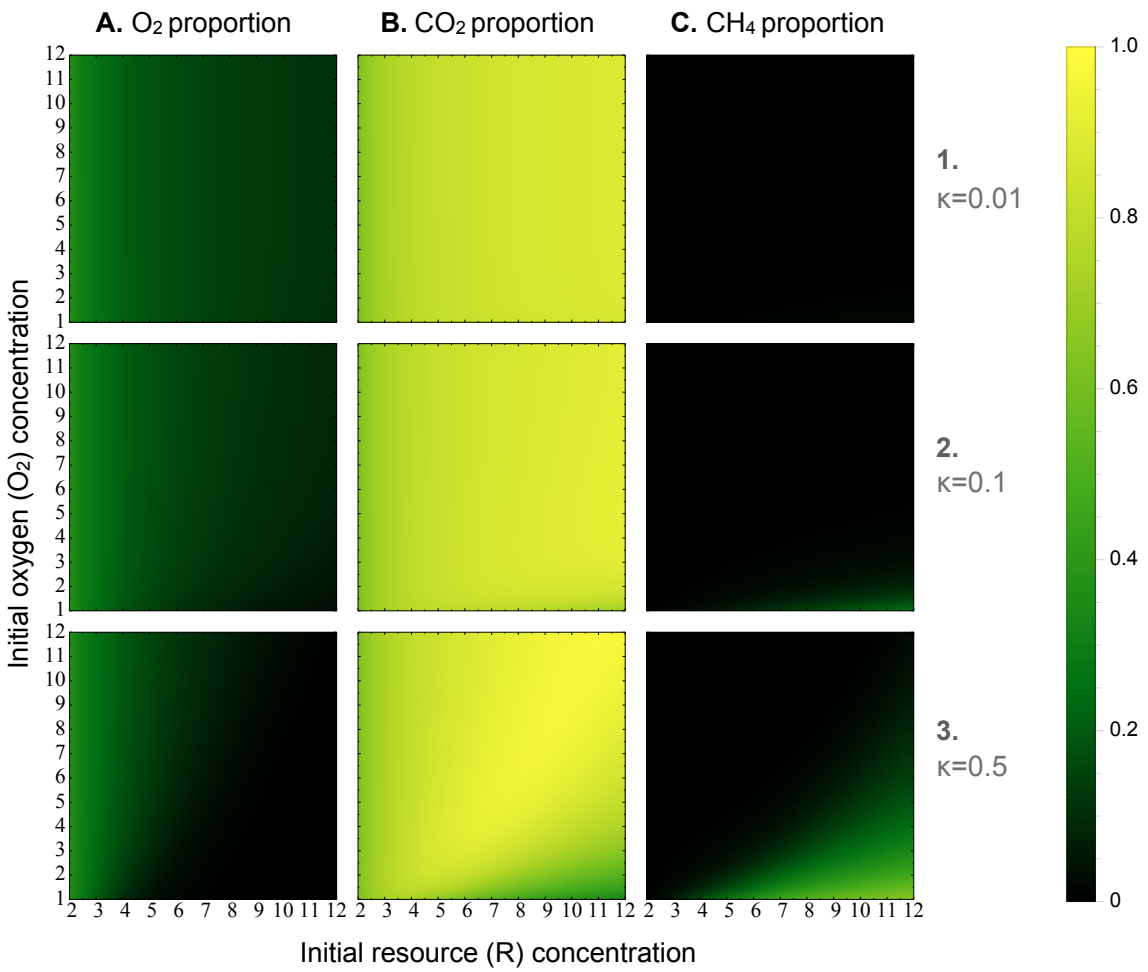

Figure S4F: Variations in O_2, CO_2, and CH_4 proportions (in columns A-C) run to steady state at set O_2 and R input values, with resource incorporation efficiency in methanogens (κ) set at 1, 10, and 50% in rows 1-3, respectively.

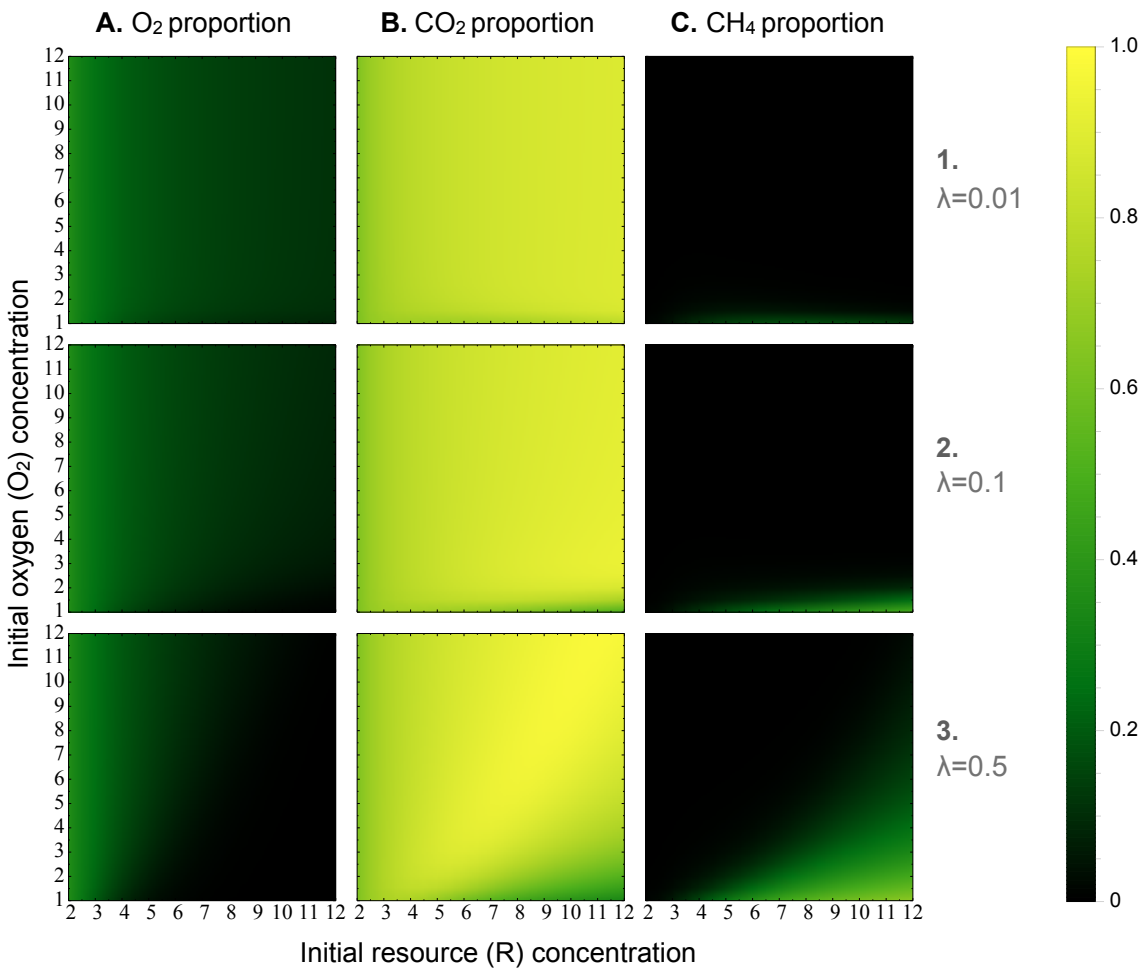

Figure S4G: Variations in O_2, CO_2, and CH_4 proportions (in columns A-C) run to steady state at set O_2 and R input values, with resource incorporation efficiency in aerobic heterotrophs (λ) set at 1, 10, and 50% in rows 1-3, respectively.

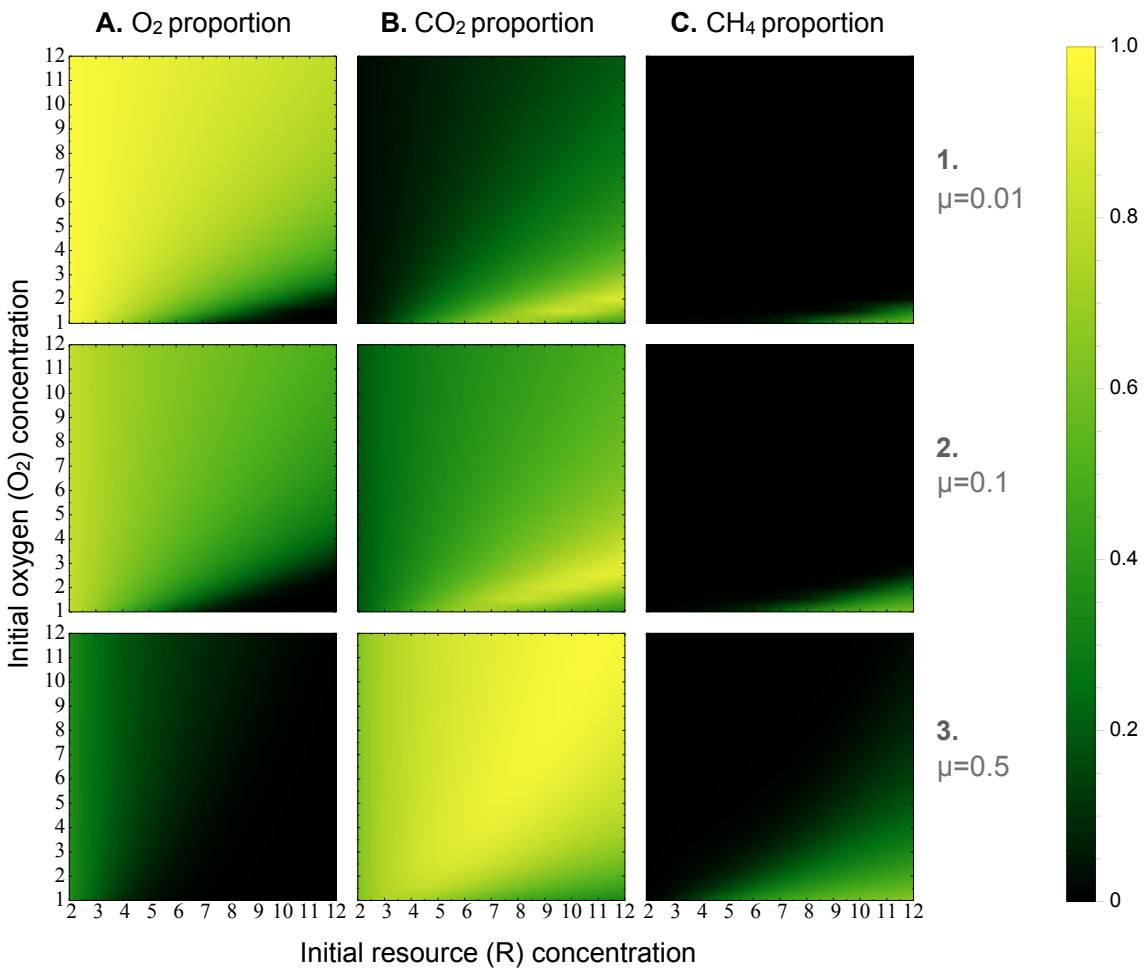

Figure S4H: Variations in O_2, CO_2, and CH_4 proportions (in columns A-C) run to steady state at set O_2 and R input values, with resource incorporation efficiency in aerobic methanotrophs (μ) set at 1, 10, and 50% in rows 1-3, respectively.

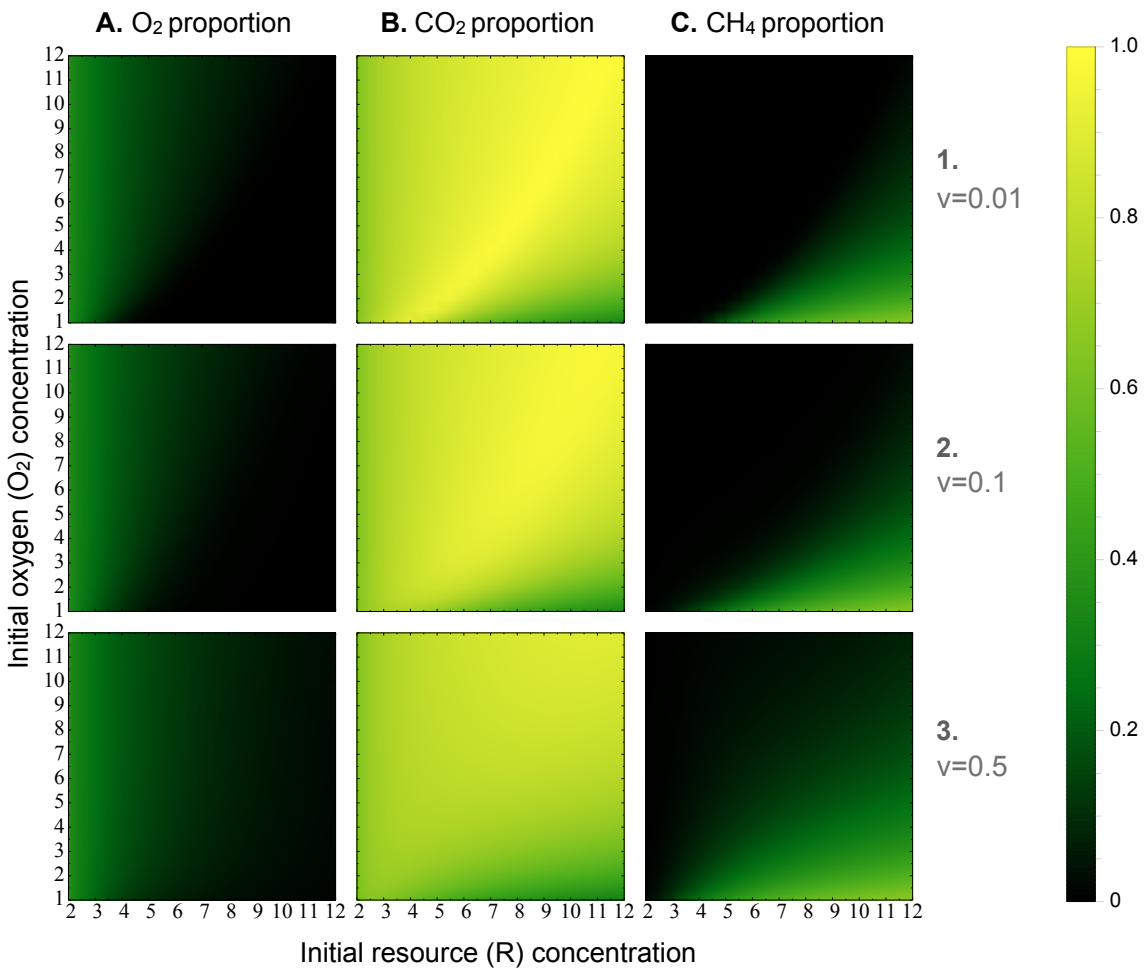

Figure S4I: Variations in O_2, CO_2, and CH_4 proportions (in columns A-C) run to steady state at set O_2 and R input values, with energy requirements of aerobic methanotrophs (v) set at 1, 10, and 50% in rows 1-3, respectively.

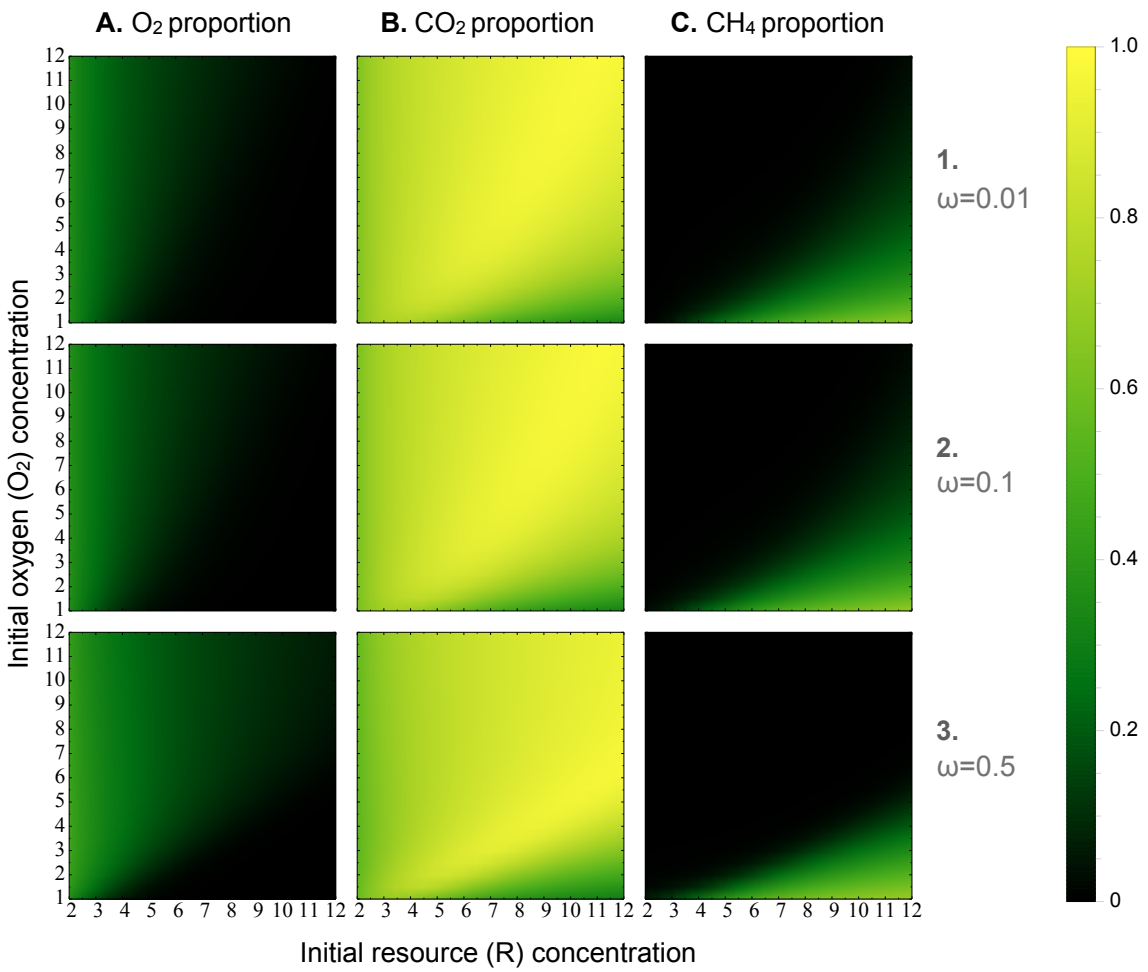

Figure S4J: Variations in O_2, CO_2, and CH_4 proportions (in columns A-C) run to steady state at set O_2 and R input values, with resource utilization efficiency in fermenters (ω) set at 1, 10, and 50% in rows 1-3, respectively.

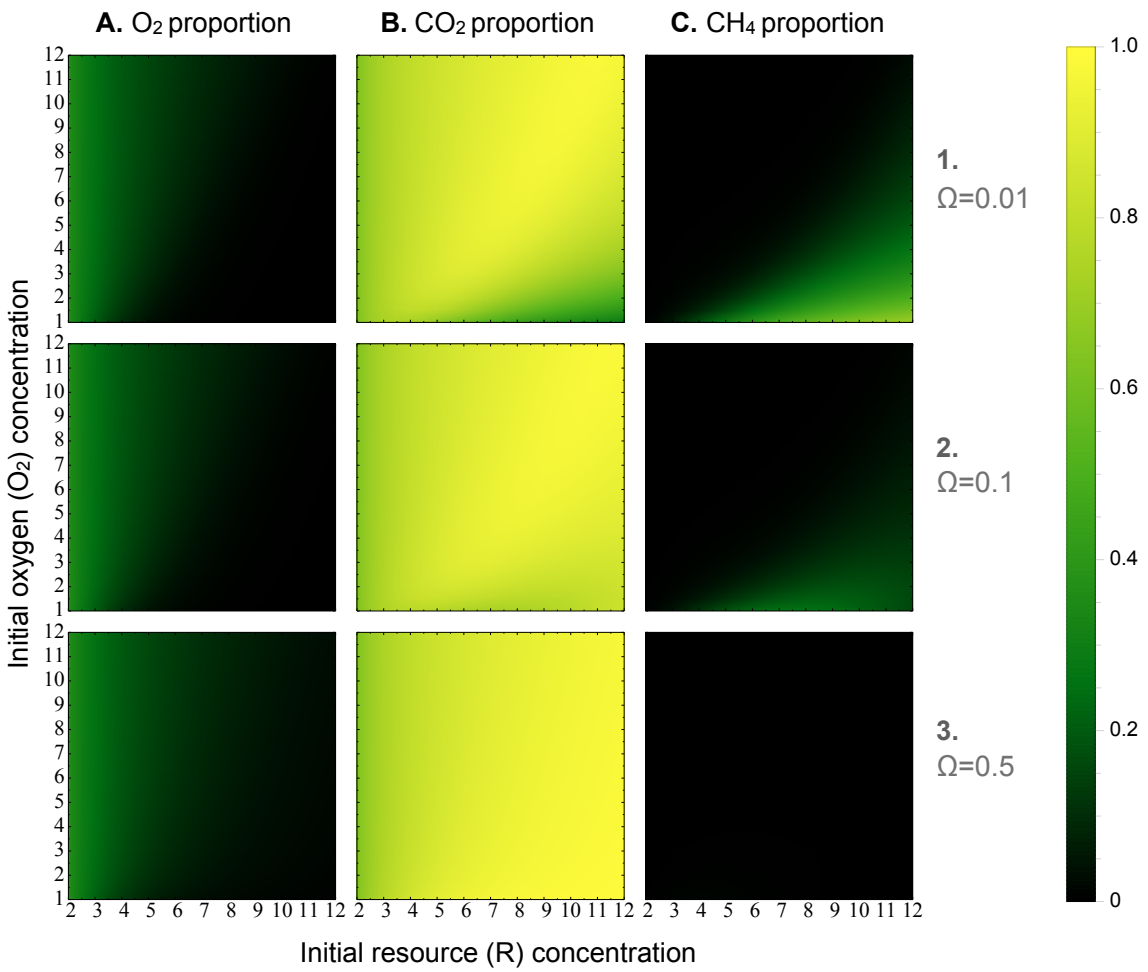

Figure S4K: Variations in O_2, CO_2, and CH_4 proportions (in columns A-C) run to steady state at set O_2 and R input values, with resource utilization efficiency in anaerobic methanotrophs (Ω) set at 1, 10, and 50% in rows 1-3, respectively.

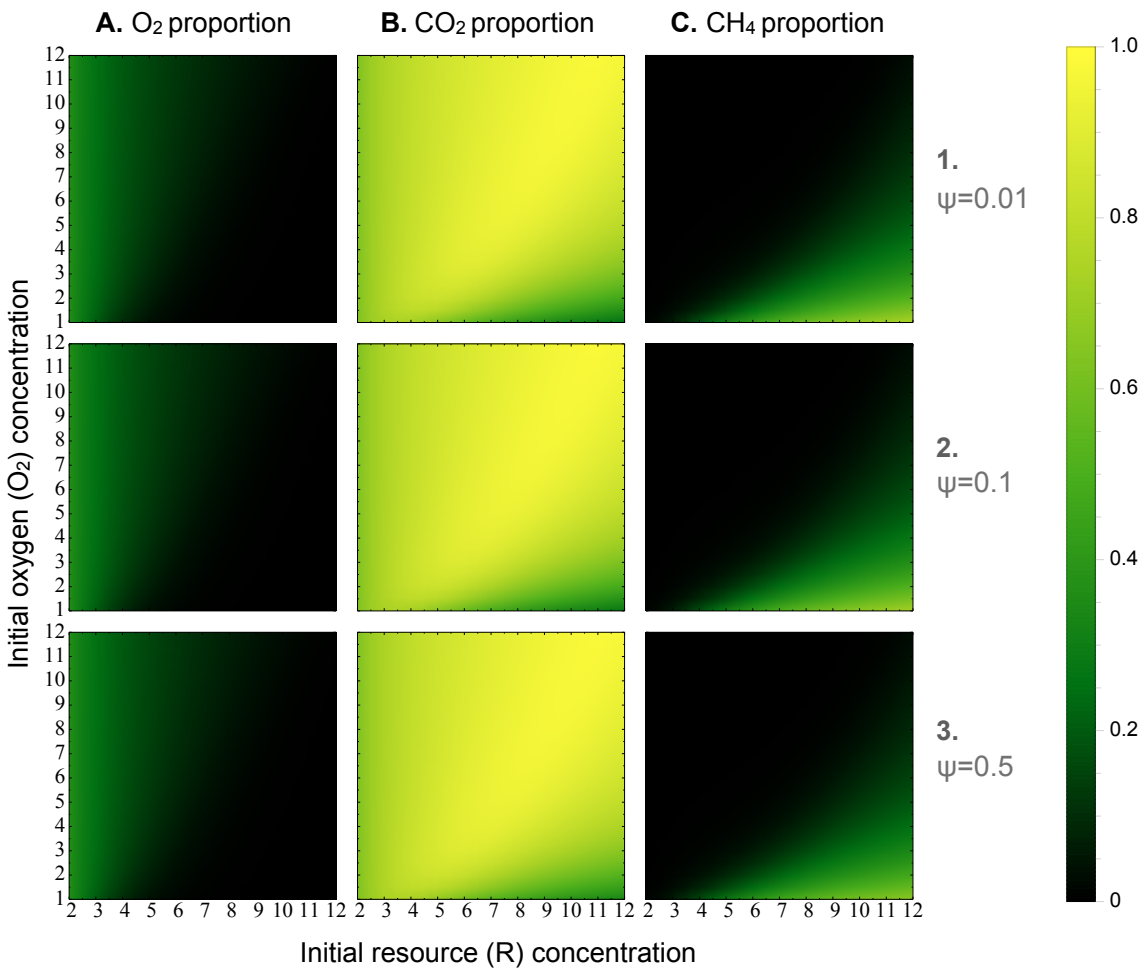

Figure S4L: Variations in O_2, CO_2, and CH_4 proportions (in columns A-C) run to steady state at set O_2 and R input values, with resource incorporation efficiency in anaerobic methanotrophs (ψ) set at 1, 10, and 50% in rows 1-3, respectively.

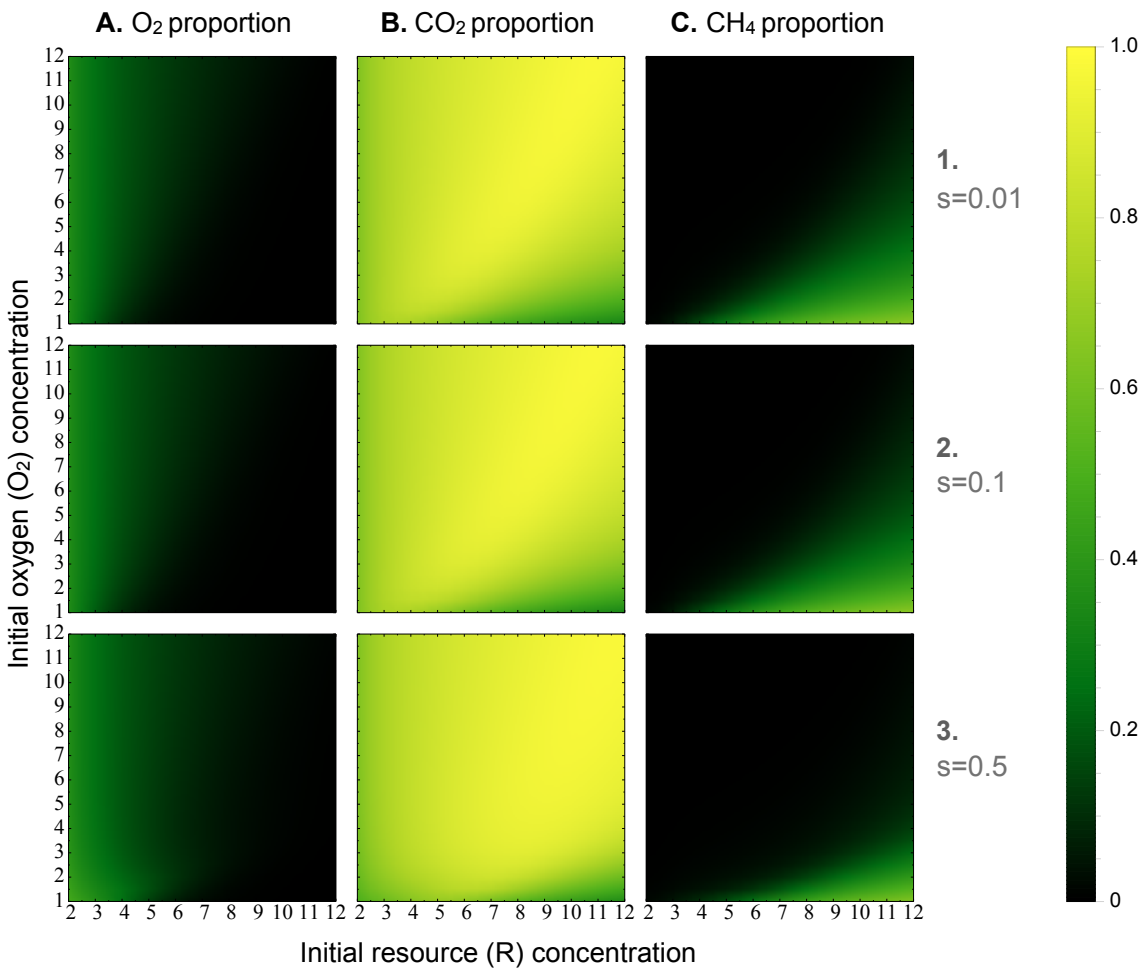

Figure S4M: Variations in O_2, CO_2, and CH_4 proportions (in columns A-C) run to steady state at set O_2 and R input values, with energy requirement for aerobic heterotrophs (s) set at 1, 10, and 50% in rows 1-3, respectively.

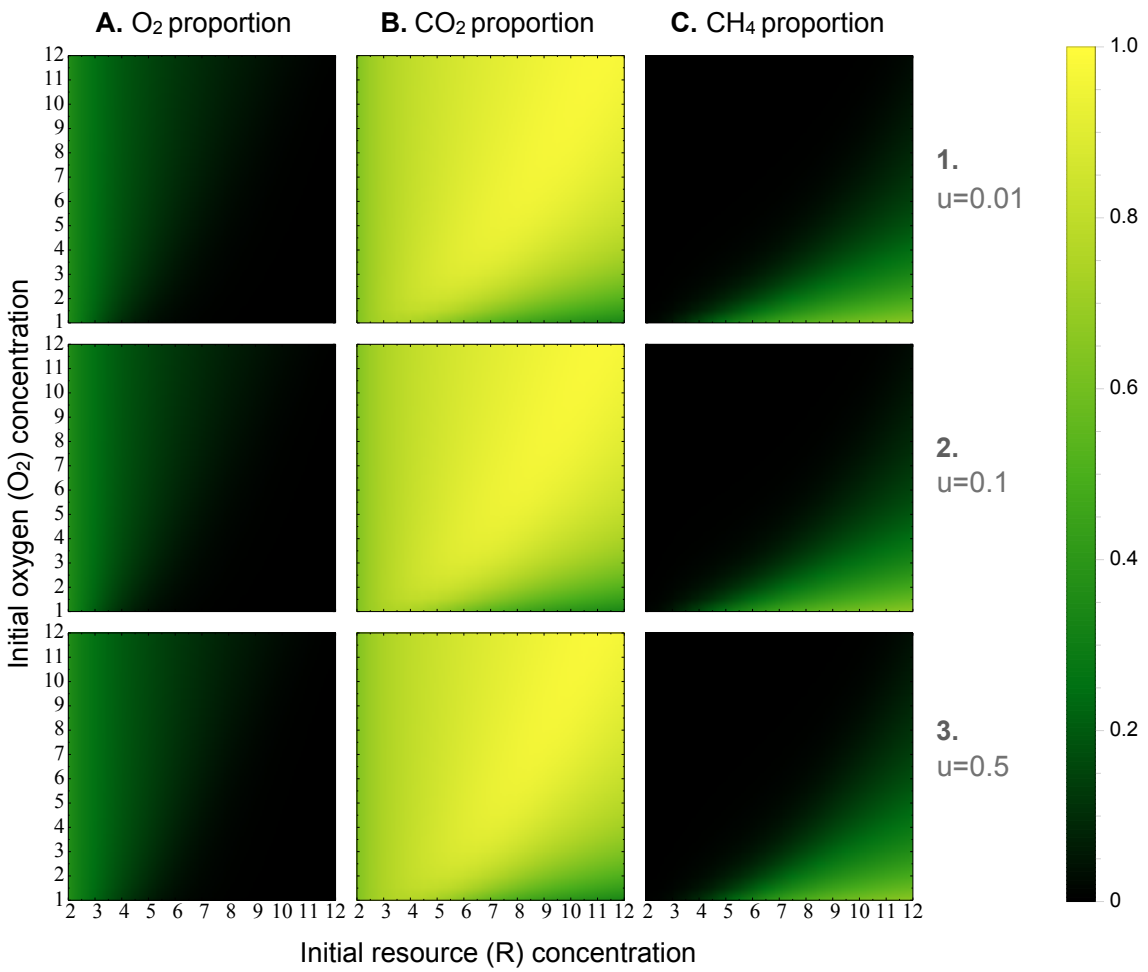

Figure S4N: Variations in O_2, CO_2, and CH_4 proportions (in columns A-C) run to steady state at set O_2 and R input values, with energy requirement for methanogens (u) set at 1, 10, and 50% in rows 1-3, respectively.

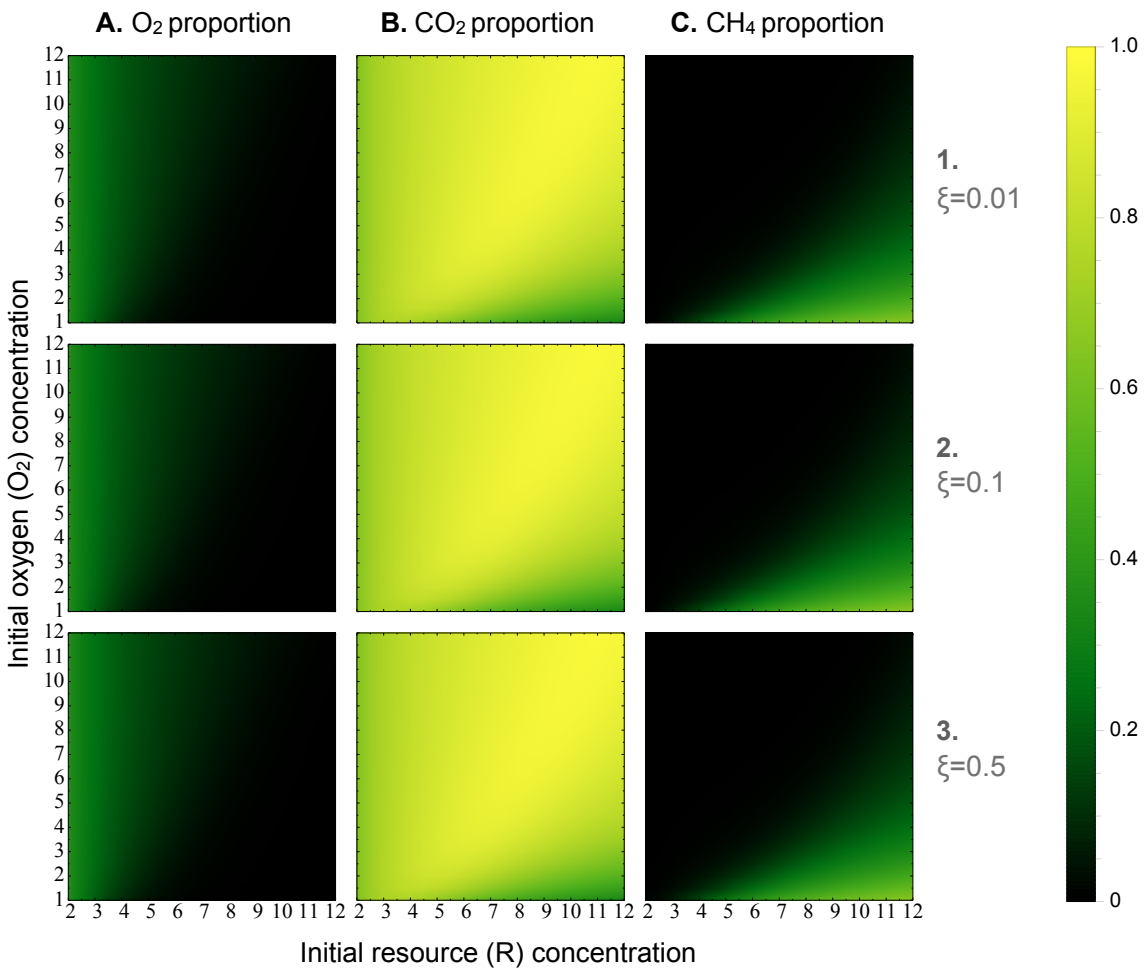

Figure S4O: Variations in O_2, CO_2, and CH_4 proportions (in columns A-C) run to steady state at set O_2 and R input values, with resource incorporation efficiency for fermenters (ξ) set at 1, 10, and 50% in rows 1-3, respectively.

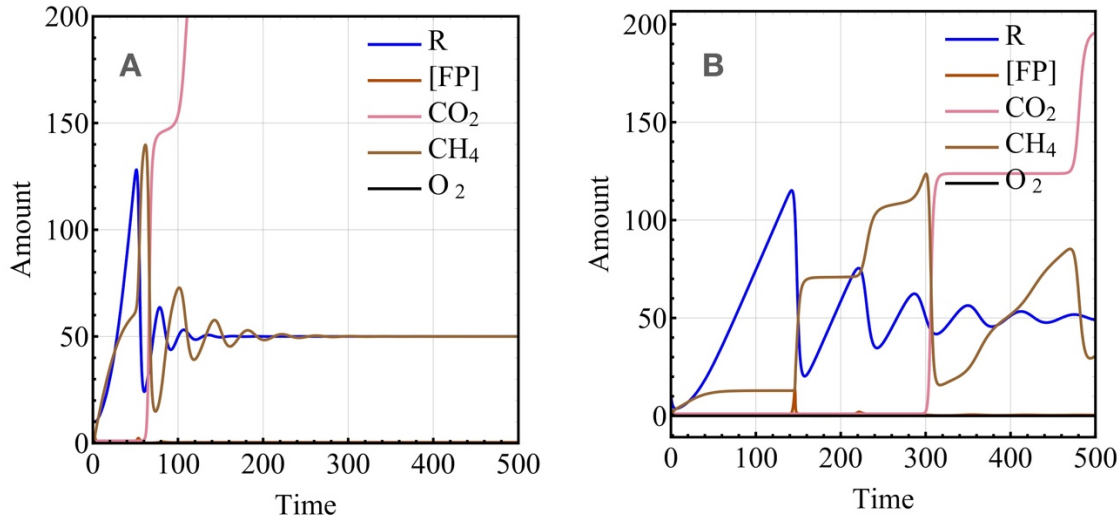

Figure S5: Long term dynamic variations in O_2, FP, and CH_4 run at two different initial O_2 concentrations, but constant input of R (resource) - (A) 5 units, (B) 1 unit. One can see that the initial O_2 concentrations affect the transient dynamics but irrespective – the system converges towards the same stable state. These dynamics are reminiscent of the complex cyclic dynamics that we would observe in the constant input of both resource and oxygen.

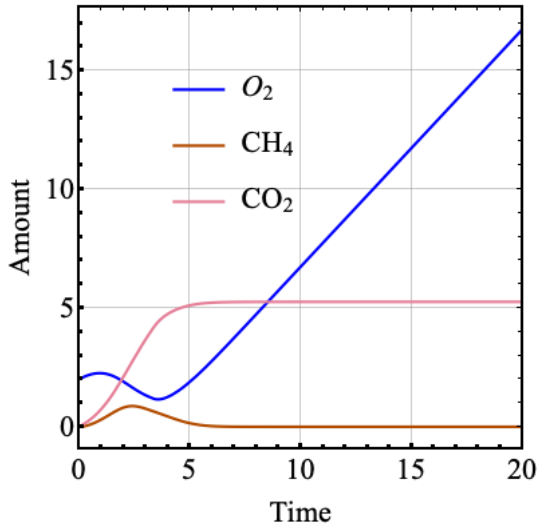

Figure S6: Dynamic variations in O_2, CO_2, and CH_4 under constant addition of O_2 and fixed initial amount of R (resource). In contrast to figure S5, due to lack of resources different populations crash and the concentration of gases/substrates (except oxygen) stabilize and as oxygen is being pumped in continually, it keeps increasing.